63-3-4

Observations

of the

CALIFORNIA INSTITUTE OF TECHNOLOGY

RADIO OBSERVATORY

Owens Valley, California

1963

1. OPTICAL IDENTIFICATION OF 3C 48, 3C 196, AND 3C 286 WITH STELLAR OBJECTS

by

T. A. Matthews and A. R. Sandage

OPTICAL IDENTIFICATION OF 3C 48, 3C 196, AND 3C 286 WITH STELLAR OBJECTS

T. A. Matthews* and A. R. Sandage**

ABSTRACT

Radio positions of the three sources have been determined with the two 90-ft antennas working as an interferometer with an rms accuracy in both coordinates better than 10 sec of arc. Direct photographs show that a star-like object exists within the error rectangle at each of the source positions. Exceedingly faint wisps of nebulosity are associated with the stars in 3C 48 and 3C 196. The observations are incomplete for 3C 286 in this regard. Photoelectric photometry of the stars shows each to have quite peculiar color indices, most closely resembling the colors of old novae, or possibly white dwarfs, but we are not suggesting identification with these types of stars. Photometry of 3C 48 through 13 months shows the star to be variable by at least $\Delta V = 0^{m}.4$. The radio flux appears to be constant. Optical spectra for 3C 48 show several very broad emission features, the most intense at $\lambda 3832$ being unidentified. Spectra by Schmidt of 3C 196 and 3C 286 show other unusual features. The radio structure of the three radio stars are similar in that each has an unresolved core of <1" diameter. However, 3C 196 and 3C 286 show halos of 12" and 20" respectively, while no radio halo has been detected for 3C 48.

It is shown that the radiant flux in the optical region can be computed from the radio flux data and the theory of synchrotron radiation for 3C 48 and 3C 196, but not for 3C 286. This, together with other arguments, suggests that the optical as well as the radio flux could be due to the synchrotron mechanism, but the arguments are not conclusive.

We have used the assumption of minimum total energy to compute the energy in relativistic particles and magnetic field required by the synchrotron mechanism to explain the observed emission. The magnetic field in each of the core components is near 0.1 gauss and depends mainly on the assumed angular size of the emitting region. The total energy in the core components is near 10^{40} ergs. The rate of radiation is such that the energy in relativistic electrons must be replaced in a time scale of a few years if the value of the magnetic field determined in this way is correct.

The frequency of occurrence of radio stars is examined and they

---

* Owens Valley Radio Observatory.

** Mount Wilson and Palomar Observatories.

are estimated to comprise from 5 to 10% of sources in the 3C catalogue. The percentage is likely to be less for fainter sources. Rough limits have been estimated for the mean distances of these radio stars. A mean distance of approximately 100 pc is suggested.

I. INTRODUCTION

One of the major programs of the Owens Valley Radio Observatory of the California Institute of Technology is the determination of precise positions of discrete radio sources. The radio observations are made with the two 90-ft antennas working as an interferometer at several spacings ranging from 200 ft to 1600 ft. The E-W direction is used to determine right ascension, and the N-S direction to find declination. The observational technique for declination measurements has been described by Read (1962) and the entire problem and results will be discussed elsewhere by Matthews and Read. Errors in determination of position in both right ascension and declination can now be made smaller than 5 seconds of arc under favorable conditions. With this high positional accuracy, the search for optical identification is now much more efficient than similar searches made several years ago, and a number of new identifications have already been made (Bolton 1960; Maltby, Matthews, and Moffet 1963; Matthews and Schmidt, unpublished).

Identifications to date by all workers have shown that radio sources are associated with galactic nebulae, supernovae remnants, and external galaxies both "normal" and peculiar. The distribution of discrete sources above $b = \pm 20^{\circ}$ is isotropic and has usually been attributed to galaxies alone. No star, except the sun, has previously been identified with a radio source. The purpose of this paper is to present evidence for the identification of three radio sources with objects which are star-like in their appearance on direct photographs, and in their photometric and spectroscopic properties.

II. RADIO AND OPTICAL PROPERTIES OF THE THREE SOURCES

Our attention was drawn to 3C 48, 3C 196, and 3C 286 as peculiar radio objects because of their high radio surface brightness. Measurements of the brightness distribution (Maltby and Moffet 1962) along both a N-S and E-W baseline at the Owens Valley Radio Observatory with a maximum baseline of 1600 wavelengths showed that these three sources are single with radio diameters of less than 30 seconds of arc. The Jodrell Bank observations of brightness distribution with four baselines from 2200λ to 61,000λ (Allen, Anderson, Conway, Palmer, Reddish and Rowson 1962) have shown that even at the longest baseline of 61,000λ, 3C 48 is unresolved in the E-W direction, which means that the radio diameter is less than 1 sec of arc E-W. Rowson (1962) has also shown that the diameter is less than 1 sec of arc in the N-S direction. However, the Jodrell Bank observations do show some structure in 3C 196 and 3C 286 in the E-W direction. The simplest two-component model fitting the E-W intensity distribution for 3C 196 is that 75% of the flux comes from a halo of about 12" diameter, while the remaining 25% of the flux is in an unresolved core of less than 1" diameter. For 3C 286, 40% of the flux comes from a halo of diameter $\sim$20", and the re-

maining 60% is again in an unresolved core of diameter less than 1". We are indebted to H. P. Palmer for the data prior to publication, upon which these diameters are based.

These small radio diameters together with the large observed radio flux initially suggested that the three sources might be additional examples of distant galaxies of large red shift such as 3C 295, which shows a similar radio surface brightness. Consequently, when precise radio positions were available, direct photographs were made of each field with the 200-inch telescope in the near red spectral region (103a E plates plus Schott RG1 filter).

The first object studied was 3C 48 (Matthews, Bolton, Greenstein, Münch, and Sandage 1961). A direct plate was taken on September 26, 1960, with every expectation of finding a distant cluster of galaxies, but measurement of the plate gave the unexpected result that the only object lying within the error rectangle of the radio position was one which appeared to be stellar. The stellar object was associated with an exceedingly faint wisp of nebulosity running north-south (surface brightness ~23 mag/arcsec^2 in V) and measuring 12" by 5" (N-S x E-W). The stellar object lies about 3" north of the center of the nebulosity. The peculiarity of the nebulosity, together with the excellent agreement between the radio position and the optical object, made it almost certain that an identification had been achieved. But the nature of the optical source remained in doubt because in late 1960 the existence of radio stars was not generally considered a serious possibility.

Two spectrograms were taken with the prime focus spectrograph at the 200-in. on October 22, 1960. One covered the blue-green region from λ3100 to λ5000 with a dispersion of 400 A/mm. The other covered the region from λ3100 to about λ7000 on an Eastman 103a F plate with a dispersion of 800 A/mm. The blue-violet spectrum is extremely peculiar, the only prominant features being several strong, very broad emission lines. The three strongest occur at λ4686 (intensity 4), λ4580 (2) and λ3832 (6). The broad emission line at λ3832 is the most striking feature and as yet has not been identified. The most obvious identification of the λ4686 line is with He II. If this is correct, then the measured wavelength of λ4686.2 ± 1 shows that the radial velocity of the object must be less than 100 km/sec. The lines could not be identified with any plausible combination of red-shifted emission lines. The total width of the two strongest lines at half intensity points is about 22 Å for λ4686 and about 30 Å for λ3832. The half, half-widths, expressed in km/sec, would indicate a velocity field (either random or systematic) within which the emission lines are formed of about 1200 km/sec for the λ3832 line, and 700 km/sec for the λ4686 line. No strong emission lines are present in the red although several faint ones do exist. In particular, Hα is definitely absent. Spectrograms of higher dispersion were subsequently obtained by Greenstein and Münch and a complete discussion of the spectroscopic features will be given by them.

Photometric observations of the 3C 48 optical object confirm its peculiar nature. On October 23, 1960, the photometry gave V = 16.06, B-V= 0.38, U-B = -0.61, colors which are similar but not identical to

old novae (Walker 1957), and to some white dwarfs (Greenstein 1958), but are quite different from ordinary stars and galaxies. This point will be discussed later in this section.

An effort was made in the case of 3C 48 to resolve the optical image. On a night of good seeing a series of exposures ranging from 10 minutes to 15 seconds was made at the 200-in. prime focus (scale = 11.06 arcsec/mm) on Eastman 103a 0 plates. On the shortest exposure plate (15^s) the image diameter of 3C 48 was measured to be 0.09 mm, which corresponds to 1" arc. This is the same diameter as images of stars of the same apparent brightness on the plate. The image of 3C 48 on all plates is sharp and appears to be stellar.

A second epoch Sky Survey plate was taken by W. C. Miller on January 18/19, 1961, with the 48-in. Schmidt to check for a detectable proper motion. This plate was centered identically with the base plate O 30 of the original Sky Survey taken on December 21/22, 1949, giving an 11-year interval. Inspection of the two plates in a blink comparator showed no detectable proper motion relative to neighboring comparison stars. The proper motion is less than $0''.05$/yr (a value which could have been detected by this method).

Optical photometry of 3C 48 continued sporadically during 1961 with the results given in Table 1. The most striking feature of these data is that the optical radiation varies! Unfortunately our time resolution is very poor. The only evidence for short term fluctuations is the data obtained on October 11/12, 1961, where the observations listed were made in a time interval of 15 minutes. We believe that the observed difference in intensity between these times is probably real because the local standard star D (see Fig. 2) was observed after each of the 3C 48 observations. The differences between the measurements of D were only $\Delta V = 0^m.007$, $\Delta(B-V) = 0^m.007$ and $\Delta(U-B) = 0^m.010$, whereas the 3C 48 differences are $\Delta V = 0^m.044$, $\Delta(B-V) = 0^m.053$ and $\Delta(U-B) = 0^m.024$.

The probable errors for most of the data of Table 1 are less than $\pm\ 0^m.02$ except for the 60" telescope data of November 19/20, 1960, where the error is $\pm\ 0^m.04$. We therefore conclude that the night-to-night variations and those over the 13-month interval are undoubtedly real. It remains for future observations to determine if short-term fluctuations with a time scale of minutes exist in the optical radiation similar to those found and studied in old novae by M. Walker (1954, 1957). The work of Smith and Hoffleit (1961) shows that there has been no large systematic variation in the magnitude of 3C 48 over the last 60 years.

Special observations for the constancy of the radio flux at 1420 Mc/s were made at the Owens Valley by K. Kellermann for more than a week in February 1962, to see if similar fluctuations are present in the radio flux data. No variation greater than 3% was detected, the probable error of a single observation being about 1.2%. Comparison with flux levels determined four months earlier showed no variation within the probable error of about 5%. Although the data are not conclusive, our present data suggest that the radio flux of 3C 48 is con-

stant while the optical flux varies by at least a factor of 1.4 in an interval of 13 months.

Following the identification of 3C 48, the other two sources were found in the same way. For both 3C 196 and 3C 286, the only objects on the direct photographs within the error rectangles have a stellar appearance. Furthermore, the stellar object in the position of 3C 196 is also associated with an exceedingly faint wisp of nebulosity which appears as a tail in position angle 120° on the stellar image. The wisp is slightly curved and has dimensions of only 3" x 1" so it is smaller than the nebulosity associated with 3C 48. The nebulosity near 3C 196 is extremely difficult to see on a 103a D plate behind a GG 11 filter exposed for 50 minutes, but is easily seen on a plate taken for us by W. A. Baum on 103a E emulsion behind red plexiglas for 60 minutes. We have no plates of 3C 48 taken on 103a D emulsion for comparison, but on a 103a F plate behind Schott RG2 (126m exp) and on a 103a E + Schott RG2 (90m exp) as well as on several 103a O plates, the 3C 48 nebulosity is visible and stronger than that associated with 3C 196. We have not detected nebulosity around 3C 286, but again the only available plate is a 103a D + GG 11 which, in view of the extreme difficulty of detecting the wisp in 3C 196 with this emulsion and filter combination, does not allow us to conclude that 3C 286 has no nebulosity.

The colors and magnitudes of the stellar objects at the radio positions of 3C 196 and 3C 286 were measured photoelectrically with the 200-in. and were found to be quite unusual, as was 3C 48. The available data, determined on only one night for each, are listed in the last two lines of Table 1. The colors of all three sources are plotted in Fig.1, which also shows three solid lines: (C) the normal main sequence relation for luminosity class V stars, (B) black body radiators and (A) objects whose energy distribution per unit frequency interval is of the form $F(\nu) \propto \nu^{-n}$. Lines are marked on curve A for various n values ranging from n = 0.0 to n = 2.0 in steps of 0.2. This form of the energy spectrum is that predicted for synchrotron radiation under certain conditions as explained in Section III. The lines B and C were computed by the methods of Appendix A. The black body line differs slightly from that computed by Arp (1961) for reasons explained in Appendix A. Note that the three radio sources fall close to line A. The only other known stellar sources in this general region of the diagram are old novae (Walker 1957, Table 1) and a very few white dwarfs. Most white dwarfs fall on or below the black body line. Those old novae which do not have composite spectra are plotted as crosses in Fig. 1 to illustrate the point. We are indebted to R. Kraft for unpublished spectral data on the old novae.

M. Schmidt has obtained spectra of both 3C 196 and 3C 286 and their spectral peculiarities again confirm that we are dealing with unusual stellar objects. Schmidt reports that at a dispersion of 400 Å/mm, 3C 196 has a continuous spectrum with no prominent features either in emission or absorption (contrary to 3C 48). He also reports (1962a) from several spectrograms that 3C 286 has a spectrum showing one emission line and possibly one absorption feature. The observed features are not the same as those observed in 3C 48.

Finally, a second epoch Sky Survey plate of 3C 286 was obtained with the 48" Schmidt on April 6/7, 1962, by J. Berger. Comparison in the blink comparator with the base Survey plate O 131 taken on June 5/6, 1950, showed that 3C 286 has no detectable proper motion over the 11-year interval. This puts an upper limit to the motion of 0".05/yr.

Table 2 summarizes the radio and optical position measurements now available for these three sources. The quoted radio positions are those which were determined before the optical identifications were made. The radio right ascension measurements are due to T. A. Matthews, the radio declination measurements are due to R. B. Read (1962). After the preliminary measurements of the 200" plates for optical position were made by Matthews to identify the stars, the final measurements of the plates were done by R. F. Griffin and the precise optical positions of Table 1 are due to him. The agreement between the radio and optical positions is excellent and strongly substantiates the reality of the identifications. The quoted errors of Table 2 are rms values.

Figures 2, 3 and 4 are finding charts for the optical objects. In Fig. 1 for 3C 48 the two photometric comparison stars B and D are shown. They have been used as local standards in the photometry done after August 17/18, 1961, and have adopted values for star B of V = 13.53, B-V = 0.50, U-B = 0.00; and for star D of V = 14.54, B-V = 0.66, U-B = 0.05. Local standards will be determined around 3C 196 and 3C 286 in the future when these objects are followed more closely.

III. POWER SPECTRUM DATA

a) The Radio Data

We have compiled and tabulated the available radio flux data for the three sources in Tables 3, 4 and 5. The measurements are from many sources, either in the literature, or from unpublished data from the Owens Valley Radio Observatory generously made available by Kellermann and Bartlett. The references are listed at the bottom of Table 5. The flux values are in units of 10^{-26}watts(meter)$^{-2}$(c/s)$^{-1}$ and have been taken directly from the various authors with no attempt to put the various absolute calibrations on a strictly homogeneous system. The power spectra in the radio range from 160 Mc to 3200 Mc are shown in Figures 5, 6 and 7. Probable errors are given in the tables where known. As a guide, the size of a 10% probable error is shown in Figures 5, 6 and 7.

The data are most complete for 3C 48, and it is evident from Fig. 5 that no single straight line can be drawn through all the points. The best compromise single spectral index which satisfies all of the points except the three in the 3000 Mc region is -0.59. Since these three high frequency observations carry so much combined weight, we conclude that a single spectral index is not acceptable. We have arbitrarily fitted segments of two power laws to the data with indexes $n_1 = -0.47$ for frequencies lower than $\nu = 7 \times 10^8$ c/s and $n_2 = -0.67$ for $\nu > 7 \times 10^8$ c/s. Kellermann, Long, Allen, and Moran (1962), using unpublished low frequency flux measurements, believe that the low frequency spectral index is even flatter than n = -0.47. They have sug-

gested that a high energy cut-off is responsible for the curvature seen in the radio spectrum. However, in view of the optical data to be discussed later, we wish to suggest that it might be interpreted as the low energy cut-off of the electrons producing the synchrotron radiation. The possibility of a low frequency cut-off is not discussed further here because of the limited observational data.

The index -0.67 fits the 3C 48 radio data for $\nu > 7 \times 10^8$ c/s quite well and we shall see later in this section that an extension of $F(\nu)$ into the optical region using the synchrotron radiation theory with $n = -0.67$ predicts the observed optical flux with remarkable accuracy.

Fig. 6 shows that the data for 3C 196 also cannot be well represented by a single spectral index, although most of the points (except the three near ν = 3000 Mc/s) do fall near the dashed line of index -0.67. We shall show later that the optical data, if all of the observed optical flux is assumed to be due to synchrotron radiation, require $n = -0.74$, and this is shown as a solid line in Fig. 6 for $\nu > 4 \times 10^8$ c/s. The behavior of the flux at low frequencies is not well determined; one suggestion is shown by the dash-dot line.

The few data available for 3C 286 suggest that the radio spectral index has the very low value of $n = -0.28$, but more observations at low and high frequencies are needed to confirm the result. Recent flux data below 400 Mc/s measured at Cambridge suggest that the spectrum of 3C 286 also flattens at the low frequency end (Conway, Kellermann and Long 1962).

b) The Optical Data

The U, B, V values of Table 1, Section II, have been converted to absolute flux units by the methods of Appendix B and have then been compared with the radio data. For 3C 48 we have adopted mean values V = 16.20, B-V = 0.40, U-B = -0.59 for this comparison, rather than treating each of the observations separately. We were fortunate in asking W. A. Baum to measure UBV magnitudes of 3C 48 during his Palomar run in December 1961, because in addition to these three colors, he measured the star in his eight-color system which extends from 3700 Å to 9800 Å and he has made these data available to us for discussion.

Table 6 summarizes the available optical data. The effective frequencies for the UBV observations are directly computed from the effective wavelengths worked out in Appendix B and given in Columns 4, 5 and 6 of Table B1 for different values of the effective index n. The value of n was estimated for each of the three sources from their observed B-V values by comparing them with Column 3 of Table B1. Baum's data were converted to absolute units by force fitting them, over the frequency interval in common, to the absolute calibration of the U, B, V points given in the first three rows of Table 6. The flux unit in Table 6 is 10^{-29} W m^{-2}(c/s)$^{-1}$.

The radio and optical data are plotted together in Fig. 8. The straight line with its family of termination curves A, B, and C is, under certain conditions (see below), the theoretical power spectrum

for an assemblage of relativistic electrons whose number in energy range E to E + dE is

$$N(E)\,dE = K\,E^{-\beta}\,dE \tag{1}$$

for $E_1 < E < E_2$ where E_1 and E_2 are the low and high energy cut-offs. The well known theory of synchrotron radiation, summarized by Oort and Walraven (1956), by Woltjer (1958), by Burbidge (1956) and others, predicts the power at frequency ν radiated by the electron assemblage to be of the form

$$F(\nu) = 1.171 \times 10^{-22}\, K\, H_\perp^{(\beta+1)/2}\, L^{(\beta-1)/2}\, \nu^{-(\beta-1)/2} \int_{\alpha_1}^{\alpha_2} \alpha^{(\beta-3)/2} F(\alpha)\,d\alpha \tag{2}$$

in units of ergs sec^{-1} cm^{-2} $(c/s)^{-1}$. $H_\perp$ is the component of the magnetic field strength perpendicular to the velocity vector of the electron; $L = 1.608 \times 10^{13}$ if the electron energy E is expressed in Bev, $L = 6.269 \times 10^{18}$ if E is in ergs, and α relates the frequency of observation ν with the low and high critical frequencies ν_1 and ν_2 by

$$\alpha_1 = \frac{\nu}{\nu_1}\,; \quad \alpha_2 = \frac{\nu}{\nu_2} \tag{3}$$

where the critical frequencies are given by

$$\nu_1 = L\,H_\perp\,E_1^{\,2}\,; \quad \nu_2 = L\,H_\perp\,E_2^{\,2}\,. \tag{4}$$

The function $F(\alpha)$ has been tabulated by Vladimirsky (1948), by Oort and Walraven (1956), and by Westfold (1958). In the following calculations we shall assume that the low frequency cut-off ν_1 is below 10^7 c/s. To compute the theoretical flux for frequencies greater than 10^8 c/s, we can put $\alpha_1 = \infty$ with good accuracy. In what follows we also put $H_\perp$ equal to a constant and thereby ignore the possibility of magnetic field gradients. Such gradients will give a different $F(\nu)$ distribution from the constant H model, as will a model such as has been postulated for the Crab (Oort and Walraven 1956), where different regions of the source contain electrons of different energies. Under these assumptions equation (2) becomes

$$\begin{aligned} F(\nu) &= D\,\nu^{-(\beta-1)/2} \int_{\alpha_2}^{\infty} \alpha^{(\beta-3)/2} F(\alpha)\,d\alpha \\ &= D\,\nu^{-(\beta-1)/2}\, I(\alpha_2) \end{aligned} \tag{5}$$

where D is a constant and where

$$I(\alpha_2) = \int_{\alpha_2}^{\infty} \alpha^{(\beta-3)/2} F(\alpha)\, d\alpha \quad . \qquad (6)$$

If the frequency of observation ν is far enough removed from the high frequency cut-off (i.e. $\alpha_2 \leq 0.01$ or $\nu_2 \geq 100\ \nu$), then the theoretical energy spectrum will be a power law of index $(\beta-1)/2$, in good general agreement with Figures 5, 6 and 7.

If we now require that all the optical flux of 3C 48 is synchrotron emission alone, then Fig. 8 shows that the high frequency cut-off, ν_2, is near 10^{15} c/s since the optical points are fainter than the extrapolated $\nu^{-0.67}$ relation. $I(\alpha_2)$ has been found by numerical integration of equation (6) with $\beta = 2.43$ corresponding to a spectral index -0.67.

Once the value of β is fixed, the only free parameter in equation (5) is the lower limit of the integral α_2. Curves A, B and C of Fig. 8 are predicted spectra for critical frequencies ν_2 of 3×10^{14} c/s, 6×10^{14} c/s and 10^{15} c/s respectively. Fig. 9 shows more detailed calculations in the optical range compared with the data of Table 6. The six curves are for cut-off frequencies ranging from 4×10^{14} c/s to 10^{15} c/s. A frequency of $\nu_2 = 7 \times 10^{14}$ c/s provides a remarkably good fit to all of the data.

The detailed calculations show that deviations from the simple power law $F(\nu) \propto \nu^{-n}$ occur if the frequency of observation is closer to the critical frequency ν_2 than $\alpha_2 = 0.01$. For $\alpha_2 > 0.01$ the [log, log] plot is no longer a straight line, but over small intervals in frequency $F(\nu)$ can still be adequately represented by an "effective index n" which will be larger than $(\beta-1)/2$. Over the optical range of the U, B, V filters ($8.4 \times 10^{14} > \nu > 5.5 \times 10^{14}$) the effective index for 3C 48 is about 1.5 (rather than 0.67 which holds for $\alpha_2 < 0.01$) and this explains why the plotted point for 3C 48 in Fig. 1 lies close to and below curve A near the value for n = 1.3. It is important to note that although curve A of Fig. 1 was computed using the theoretical synchrotron power law of equation 5 with $\alpha_2 = 0$, objects which lie close to curve A are not necessarily synchrotron radiators. The close fit of observations to curve A only means that over the very small frequency range between the U and the V filters the energy distribution can be approximated by $F(\nu) \propto \nu^{-n}$ with the n appropriate to the particular position on curve A.

Finally, with regard to Figures 8 and 9 it should be mentioned that the value of the spectral index $(\beta-1)/2$ is quite critical for a good fit of the optical data. The first calculations for 3C 48 were made with an index of 0.59 as suggested by the best overall fit to the radio data of Fig. 5. The fit of those calculations to the optical data was much poorer than in Fig. 9 with deviations over the U to V interval ranging to 0^m3. Consequently, in making the fit of Fig. 9 there are in effect the two adjustable parameters β and ν_2. However, β can only be adjusted within the limits imposed by the detailed radio data of Fig. 5 and Table 3.

Similar calculations were made for 3C 196 and 3C 286 and are shown in Figures 10 and 11. In the case of 3C 196, Fig. 10 shows that equation (5) gives a satisfactory tie-in between the radio and optical data if the high frequency cut-off is about 4×10^{14} c/s. But again it should be emphasized that this does not in itself prove that the optical radiation is due to synchrotron emission. However, Figures 8 and 10 are so similar that it would be surprising if the optical emission were not somehow related to the radio flux. On the other hand, Fig. 11 shows that the situation must be more complicated for 3C 286. We can derive a curve such as B which will pass through one of the optical points (which, of course, is always possible as long as the optical flux is less than or equal to the $\nu^{-(\beta-1)/2}$ relation extrapolated from the radio region) but no change of parameters can predict the observed color of 3C 286 as we have done for 3C 48 and 3C 196. Consequently, we conclude that the optical radiation of 3C 286 is probably not due to synchrotron emission. The high frequency cut-off must occur at frequencies between 10^{11} and 10^{13} c/s and most if not all of the observed radiation from the 3C 286 star may be thermal.

In addition to the agreement of theory and observation in Figures 8, 9, 10 and 11, an indirect argument might be used to suggest that the optical flux is synchrotron radiation. The argument concerns the explanation of the fluctuations of the optical intensity of 3C 48. The time for an electron to lose one half of its original energy E (in Bev) is given (Oort and Walraven 1956) by

$$t_{1/2} = \frac{3.05}{H_\perp^2 E} \text{ days.} \tag{7}$$

The energy of the electrons which emit the large majority of the optical radiation is related to the magnetic field through equation (4), because individual electrons radiate mainly near their own critical frequency. Putting $\nu = 7 \times 10^{14}$ in equation (4) gives $E = 6.6\, H^{-1/2}$ Bev and substituting in equation (7) we have

$$t_{1/2} = \frac{0.462}{H_\perp^{3/2}} \text{ days (for } \nu = 7 \times 10^{14} \text{ c/s)} \tag{8}$$

for the decay time of electrons responsible for optical radiation. In the radio frequencies, the decay time is very much longer. If ν = 1000 Mc/s, then equation (4) requires $E = 7.9 \times 10^{-2}\, H_\perp^{-1/2}$ Bev which, from equation (7) gives

$$t_{1/2} = \frac{387}{H_\perp^{3/2}} \text{ days (for } \nu = 10^9 \text{ c/s).} \tag{9}$$

If the synchrotron radiation is steady, new electrons must be injected at or accelerated to energy E at just the rate necessary to replace electrons degraded in energy from E due to their own radiation. If this steady state is not exactly maintained, then the distribution function of equation (1) is not exactly maintained, and the radiated power will fluctuate with the time scales of equation (7). Equations (8) &(9) show the corresponding time scale of variations for the radio frequencies is 840 times longer than the optical time scale, which might

then explain why the radio flux is observed to remain constant over the same time intervals in which the optical radiation fluctuates.

The amplitude of the fluctuations will be determined by the fluctuation in the number of electrons radiating, or by any change in the mean magnetic field seen by these electrons. The number of electrons being observed by a radio receiver is 900 times the number observed by the V filter. This takes into account the electron spectrum (equation 1), the bandwidths used at the two frequencies (radio, $\Delta\nu = 2 \times 10^7$ c/s; optical, $\Delta\nu = 8.6 \times 10^{13}$ c/s) and the bandwidth into which an electron radiates at the two frequencies. About 10% of the radio electrons comes from electrons which previously radiated in the optical region, thus the presence of radio intensity fluctuations depends primarily on the constancy of the injection mechanisms at energies from 0.1 to 1 Bev. Equation (8) shows that the optical flux variation on a time scale of a day would require $H_\perp$ to be about 1 gauss and therefore the optical electrons would have an energy about 6 Bev according to equation (4).

With the synchrotron mechanism in mind we requested W. A. Hiltner to measure the optical polarization of 3C 48, which he did at the McDonald Observatory in late 1960, and he reports that any polarization is less than 2%. This negative result may mean either that the optical radiation is thermal or that the magnetic fields are sufficiently tangled so that the net polarization observed when averaged over the region of emission is immeasurably small.

IV. SOME PHYSICAL PARAMETERS EVALUATED FROM THE SYNCHROTRON THEORY

Further insight into the physical conditions that may exist in these stars can be gained by using the synchrotron mechanism to calculate the magnetic field and minimum total energy required to produce the observed radiation. In doing this, we follow the computational methods of Burbidge (1956; see also Burbidge and Burbidge 1957). Parallel calculations have been carried out assuming first that the synchrotron spectrum extends into the optical region as in Figures 8, 9, and 10, and second that the optical radiation is thermal and the high frequency cut-off occurs at $\nu_2 = 10^{10}$ c/s. The total flux emitted by the source is given by

$$L = 4\pi r^2 \int_{\nu_1}^{\nu_2} F(\nu)\, d\nu \qquad (10)$$

where r is the distance (L is not to be confused with the constant in equations 2 and 4). In making the integration the flux spectral distribution has been assumed to be of the form $F(\nu) \propto \nu^{-n}$ between the lower cut-off frequency ν_1 and the upper cut-off frequency ν_2. Using the distribution of electron energies given by equation (1) and noting that the rate of radiation of a single electron is $dE/dt = -2.368 \times 10^{-3} H_\perp^2 E^2$ ergs sec^{-1}, then

$$L = 2.368 \times 10^{-3} H_\perp^2 K \int_{E_1}^{E_2} E^2 N(E)\, dE \qquad (11)$$

where E is in ergs, L in ergs $(\text{sec})^{-1}$, $H_\perp$ in gauss.

The total energy of relativistic electrons is E_e and is given by

$$E_e = K \int_{E_1}^{E_2} E\, N(E)\, dE \ . \tag{12}$$

We also make the assumption (see Burbidge 1959) that the heavy particle energy, E_p, is 100 times the electron energy E_e.

The energy in the magnetic field

$$E_m = \frac{H^2}{8\pi} V \tag{13}$$

where V is the volume of the emitting region. If we now assume that the total energy $(E_m + E_e + E_p)$ is a minimum, then it can be shown that

$$E_m = \frac{3}{4} (E_p + E_e) \ . \tag{14}$$

From equations (1), (11), (12), (13) and (14) we can solve for the minimum total energy $E_T = E_m + E_p + E_e$ with the result that

$$E_T \text{ (min.)} = 4.586 \times 10^{17} \left[C\, L(1)\right]^{4/7} S^{9/7}\, r^{17/7} \tag{15}$$

where S is the angular diameter in arcseconds, and where L(1) is the emitted flux if the source were at a distance of one parsec. The value of C is a slow function of spectral index n, and of the upper and lower energy cut-offs, and is given by

$$C = 4.805 \times 10^{8} \left(\frac{\beta-3}{\beta-2}\right) \left[\frac{1-\left(\frac{\nu_2}{\nu_1}\right)^{-(\beta-2)/2}}{1-\left(\frac{\nu_2}{\nu_1}\right)^{-(\beta-3)/2}}\right] \ .$$

The magnetic field H which produces the minimum value of E_T is

$$H(E_T \text{ min.}) = 3.819 \times 10^{-4} \left[C\, L(1)\right]^{2/7} S^{-6/7}\, r^{-2/7} \text{ gauss.} \tag{16}$$

An interesting result of equation (16) is that the magnetic field depends almost entirely on the angular size and only slightly on the distance.

The ratio $\tau = \frac{E_e}{L}$ is a measure of the time scale of replenishment of the relativistic electrons, or of the lifetime of the source itself if no replenishment occurs. Under the assumptions that have been made, the total energy E_T is 236 times E_e.

Since we do not have any good estimate of the distance to these

sources the values of L(1), V(1), H(1), $E_T(1)$ and $\tau(1)$ are given in Table 7 for a distance of one parsec. The value of the absolute visual magnitude M_v is also given where the lower limit corresponds to assuming that all the optical radiation is thermal. Table 8 gives the various scaling factors to calculate the parameters for other distances. The angular size of 3C 48 has only an upper limit as do the cores of 3C 196 and 3C 286. In order to indicate the effects of size, the tables have been computed for two assumed sizes of 1.0 and 0.1 arcsecond.

The most interesting feature of Table 7 is the large value of magnetic field necessary in each of the radio core components. The value is almost independent of the assumed cut-off frequency, but does depend on the assumed size. The value of $H = 0.20\ S^{-6/7}\ r^{-2/7}$ gauss for 3C 48 is not far from the estimate of 1 gauss found necessary in Section IIIc to explain the observed optical intensity fluctuations; this perhaps adds further weight to the suggestions of optical synchrotron radiation.

For a mean distance of 100 pc, as is suggested in Section VI, for 3C 48 the values of total energy $E_T = 1.1 \times 10^{41}\ S^{9/7}$ erg, and of the magnetic field $H = 0.054\ S^{-6/7}$ gauss, are almost completely independent of cut-off frequency. The cores of the three objects all have similar values for these quantities. The time scale τ depends on cut-off frequency and is $\tau(\nu_2 = 10^{10}\ c/s) = 86\ S^{9/7}$ years or $\tau(\nu_2 = 7 \times 10^{14}\ c/s) = 2.4\ S^{9/7}$ years. Since S is less than 1", both of these time scales are very short and indicate either that the star must be continuously supplying relativistic electrons, or that the production of secondary electrons and the acceleration of particles are efficient processes. In either case a continuing supply of relativistic electrons must be made available on a short time scale by some process if the magnetic field we have assumed is correct. But it should be pointed out that the requirement for replenishment need not hold if we discard the requirement of minimum total energy. If the magnetic field is arbitrarily made very much smaller than computed above, τ can be made arbitrarily long because $\tau \propto H^{-3/2}$. Thus, if later investigations prove it difficult to find a continuing supply of electrons, τ can be made as long as the lifetime of the source by lowering H. Further investigation of the optical variations might show whether or not the optical radiation is indeed due to the synchrotron mechanism, and thus determine the value of H.

Table 9 gives the values of the physical parameters discussed here that might be expected for an average object at the suggested mean distance of 100 parsecs. The mean absolute visual magnitude would be $M_v = +12$.

V. AN ESTIMATE OF THE PERCENTAGE OF RADIO STARS IN THE VARIOUS CATALOGUES

a) The Strongest Radio Sources

In the 3C, Mills, and the Caltech catalogues there are 24 radio sources north of $\delta = -47^\circ$ whose flux at 958 Mc/s is greater than $19 \times 10^{-26}\ W\ m^{-2}(c/s)^{-1}$, a limit which is just below the faintest of the radio stars. This listing omits all sources which are identified with

galactic nebulosities (i.e. H II regions, supernovae remnants, etc.), or which probably belong to that class (i.e. low galactic latitude, radio diameter $\geq 3'$, or thermal spectrum). Of these 24 sources, 13 have been identified with galaxies and 3 are now identified with stellar objects, leaving 8 unidentified sources.

Two of the 8 are probably extragalactic because they have the characteristic two-component structure (Maltby and Moffet 1962) found for three quarters of all extragalactic radio sources. An additional two are also probably extragalactic for similar reasons, but the data are poorer. This leaves 4 possible candidates, which together with the 3 radio stars already known, suggests that as many as 7 out of the 24 strongest radio sources (excluding galactic nebulosities) might be radio stars. Therefore, at least 3/24 (or 12%), but less than 7/24 (or 29%) of the strongest sources which are not galactic nebulosities could be radio stars.

b) In the 3C Catalogue

The diameter measurements made by the Jodrell Bank workers (Allen et al. 1962) of 324 sources in the 3C catalogue provides another possible means of separating out more candidates. The diameter characteristics of the three known radio stars are unique in that they have a halo (probably not much larger than 30') and a considerable fraction of the radiation concentrated in an unresolved core. Including 3C 48, 3C 196, and 3C 286, there are 13 radio sources out of the sample of 324 which have the necessary diameter characteristics. None of these have been identified with galaxies. (Four other sources might also be included, but the information is not complete enough to decide if they fulfill all the criteria.) These 13 (or possibly 17) sources suggest that about 4% (or possibly 5%) of that portion of the 3C catalogue which has been surveyed for angular diameter could be radio stars. This percentage is a lower limit because it depends on the degree of completeness of the 3C catalogue at low galactic latitudes where the effects of confusion and uneven background variations are strongest. Of course we are certain that the absolute lower limit to the percentage of radio stars in the catalogue is 1%, obtained from the three known stars out of a sample of 324.

The question now arises whether these estimates of the percentage of radio stars made above are in contradiction with the findings of the Cambridge group (Scott, Ryle, and Hewish 1961; Ryle and Clarke 1961) that less than 1% of the sources brighter than $\sim 10^{-27}$ W m^{-2} (c/s)$^{-1}$ at 178 Mc/s can be halo objects in the Galaxy. The special Cambridge observations were made in two selected regions toward and away from the hemisphere containing the galactic center (Scott et al. used $l^{II} \sim 120°$, $b^{II} \sim -54°$ and $l^{II} \sim 300°$, $b^{II} \sim +63°$; Ryle and Clarke used $l^{II} \sim 146°$, $b^{II} \sim -50°$ and $l^{II} \sim 330°$, $b^{II} \sim +59°$ and separated by about 180° on the plane of the sky. If an appreciable number of the faint sources detected in that study had been in the galactic halo, then a marked difference in the number of sources in these two directions would have been found because of the different volumes of the galactic halo surveyed. No difference was observed greater than the statistical fluctuations of 10^4 sources per steradian to the limit of

10^{-27} W m^{-2} $(c/s)^{-1}$. Therefore, less than 1% of the radio sources to this limit can belong to the galactic halo. These findings are not in contradiction with our estimates for the following reasons. (1) Our estimate of 4% to 5% as radio stars refers to sources brighter than the limiting flux of the 3C catalogue, 8×10^{-26} W m^{-2} $(c/s)^{-1}$. It is very likely that this percentage will drop in catalogues which survey to fainter flux levels because the background count of external sources will begin to outnumber the galactic sources in the same way that galaxies outnumber stars as we photograph to faint levels in optical astronomy. (2) The Cambridge conclusion refers to objects in the galactic halo, whereas the radio stars may be concentrated toward the galactic plane and no evidence of anisotropy would then be detected by their experiment.

VI. ESTIMATE OF THE DISTANCE OF THE RADIO STARS

Two arguments may be used to show that the three radio stars identified so far are probably nearby.

a) The thirteen possible radio stars discussed in Section V have a random distribution in both latitude and longitude with no concentration toward one hemisphere of the sky. Assuming that these 13 candidates are actually radio stars, then their roughly isotropic distribution shows that they cannot be distant halo objects because, if they were, a marked asymmetry toward the hemisphere containing the galactic center would occur due to the sun's peripheral position (note e.g. the globular clusters). Therefore the radio stars must be nearby and in the galactic plane.

b) A rough upper limit to the average distance between radio stars can be estimated as follows. We shall assume that the number of radio stars in the 3C catalogue is $0.07 \times 471 = 33$ sources. This number must be corrected for the portion of the sky unobserved in the catalogue which, if the radio stars are concentrated toward the plane, gives an incompleteness factor of 1.6. There would then be about 50 radio stars in a whole sky survey carried to a flux density greater than 8×10^{-26} W m^{-2} $(c/s)^{-1}$ at 178 Mc/s. An extreme assumption which leads to a generous upper limit to the average separation is that the entire volume of the galaxy is surveyed for these stars to this flux level. Assuming a volume of 10^{11} pc^3 for the galaxy gives an average density of one radio star per 2×10^9 pc^3. If we divide the galaxy into cubical cells of length d pc on a side such that each cell contains one radio star at its center, then $d^3 = 2 \times 10^9$ pc^3 or $d = 1300$ pc. This is of the order of the average distance of any given radio star from its nearest neighbor. If the sun is equidistant between its two nearest radio stars, then the average distance between us and the nearest radio star is $d/2 = 650$ pc.

This is an extreme upper limit because we have seen that the 13 possible candidates for radio stars do not have an apparent concentration toward the galactic plane and have no asymmetry in their distribution over the sky. Thus the space occupied by these 13 sources is more likely to be a sphere whose diameter is smaller than the equivalent.

width of the galactic plane which is about 600 pc (M. Schmidt 1962b). The volume of such a sphere is 11 x 10^7 pc^3. If this contains 13 sources, then the number density is one radio star per 1.0 x 10^7 pc^3 or d = 200 pc, or r = d/2 = 100 pc as the average distance of the sun from the nearest radio star. An equally rough estimate for the lower limit to the distance is implied by the lack of detectable proper motion, less than 0".05/annum for 3C 48 and 3C 286. If the effect of standard solar motion only is considered, then the minimum distance of both objects must be near 60 pc. Any additional space motion of the stars would probably increase this minimum distance by an unknown amount.

Both of these estimates are rough and should only be taken to indicate an order of magnitude for the distance. In the calculations of Section IV we have used a mean distance to the three radio stars of 100 pc.

VII. CONCLUSIONS

The three radio sources identified here seem to be the first members of an entirely new class of objects. The physical conditions giving rise to the radio and optical radiation are almost entirely unknown. The parameters computed by the conventional synchrotron theory in Section IV lead to strange conditions such as high magnetic fields and short replenishment times for the energy stored in the electrons. If these conditions actually apply, we have "stellar" objects which are capable of accelerating high energy particles in short times (τ = E/L = years to a few 10^2 years) by an unknown process. If there are as many as 50 such radio stars in our Galaxy, these objects may be an important source for cosmic rays. Work now in progress on additional identifications should lead to a significantly larger sample for study.

ACKNOWLEDGMENTS

We wish to express our appreciation to the many people who have let us use their unpublished material. In particular, we would like to thank Baum and Hiltner for their photoelectric photometry, Greenstein and Schmidt for information of the spectra, Griffin for his accurate optical positions, Read for his precise radio declinations, Kellermann and Bartlett for their radio flux data, and Palmer for letting us use the Jodrell Bank data at large spacings before publication. We have also had useful discussions with Greenstein and Schmidt and we wish to express our appreciation to them.

The Radio Astronomy program at the California Institute of Technology is supported by the United States Office of Naval Research under Contract Nonr 220(19).

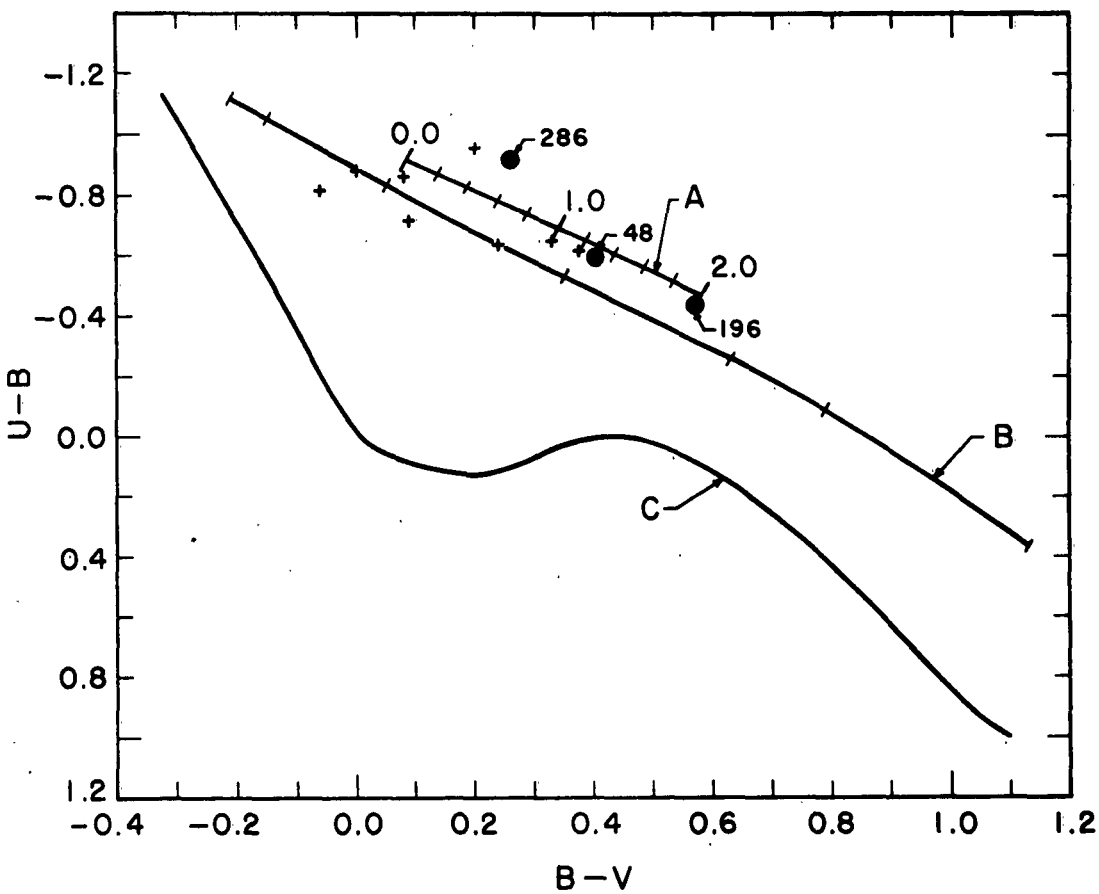

Figure 1. The two color diagram for various types of objects. Line C is for unreddened main sequence stars, line B is for black body radiation, and line A is for sources whose energy distribution is of the form $F(\nu) \propto \nu^{-n}$. Values of n from 0.0 to 2.0 are marked along curve C. Colors for the three radio stars are plotted as filled circles. Colors for a few old novae are shown as crosses. The tics on curve B indicate values tabulated in Table A3.

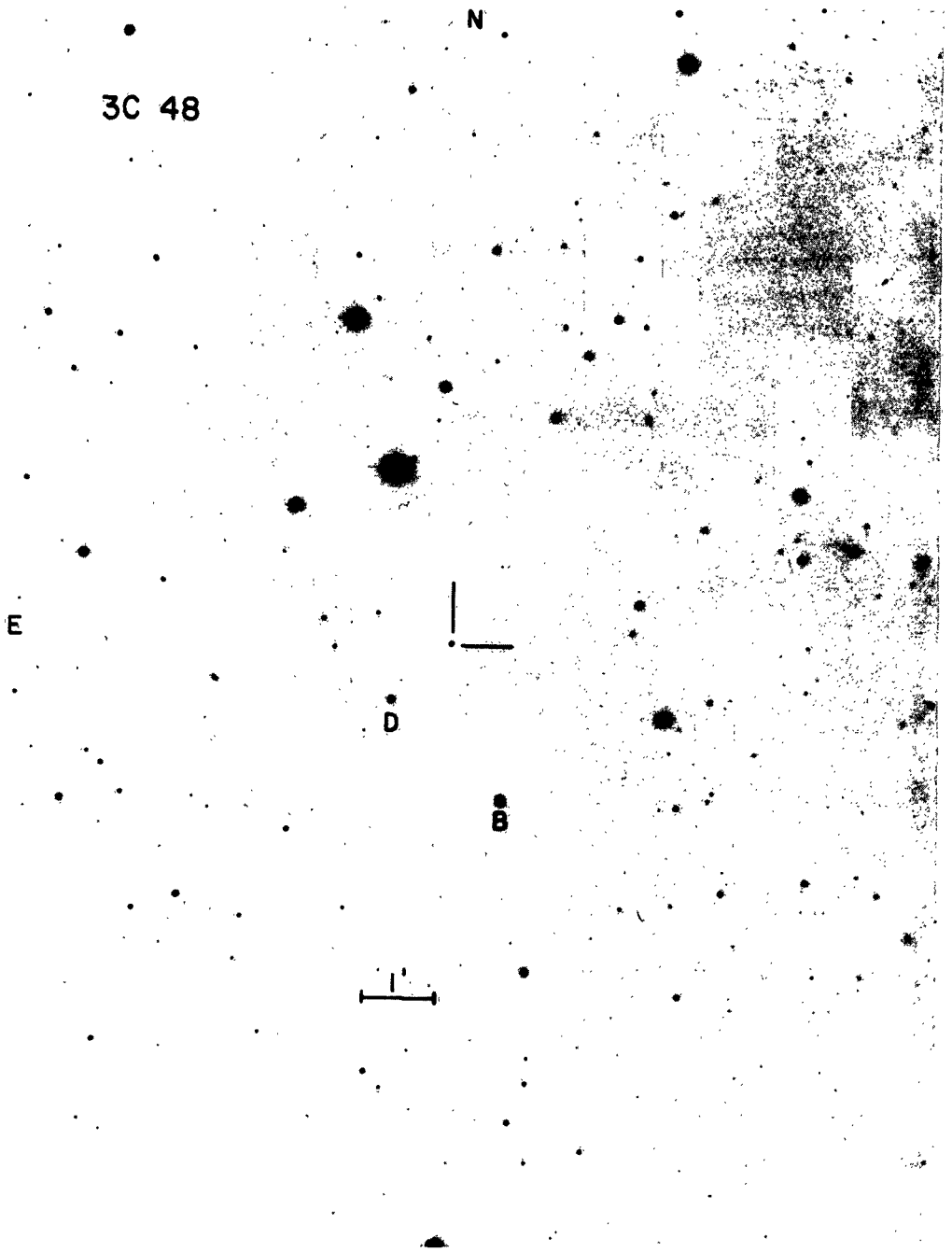

Figure 2. Finding chart for 3C 48 taken from a 10^m exposure with the 200-inch. Local photometric standard stars B and D are marked. The data are V = 13.53, B-V = 0.50, U-B = 0.00 for star B; V = 14.54, B-V = 0.66, and U-B = 0.05 for star D.

Figure 3. Finding chart for 3C 196.

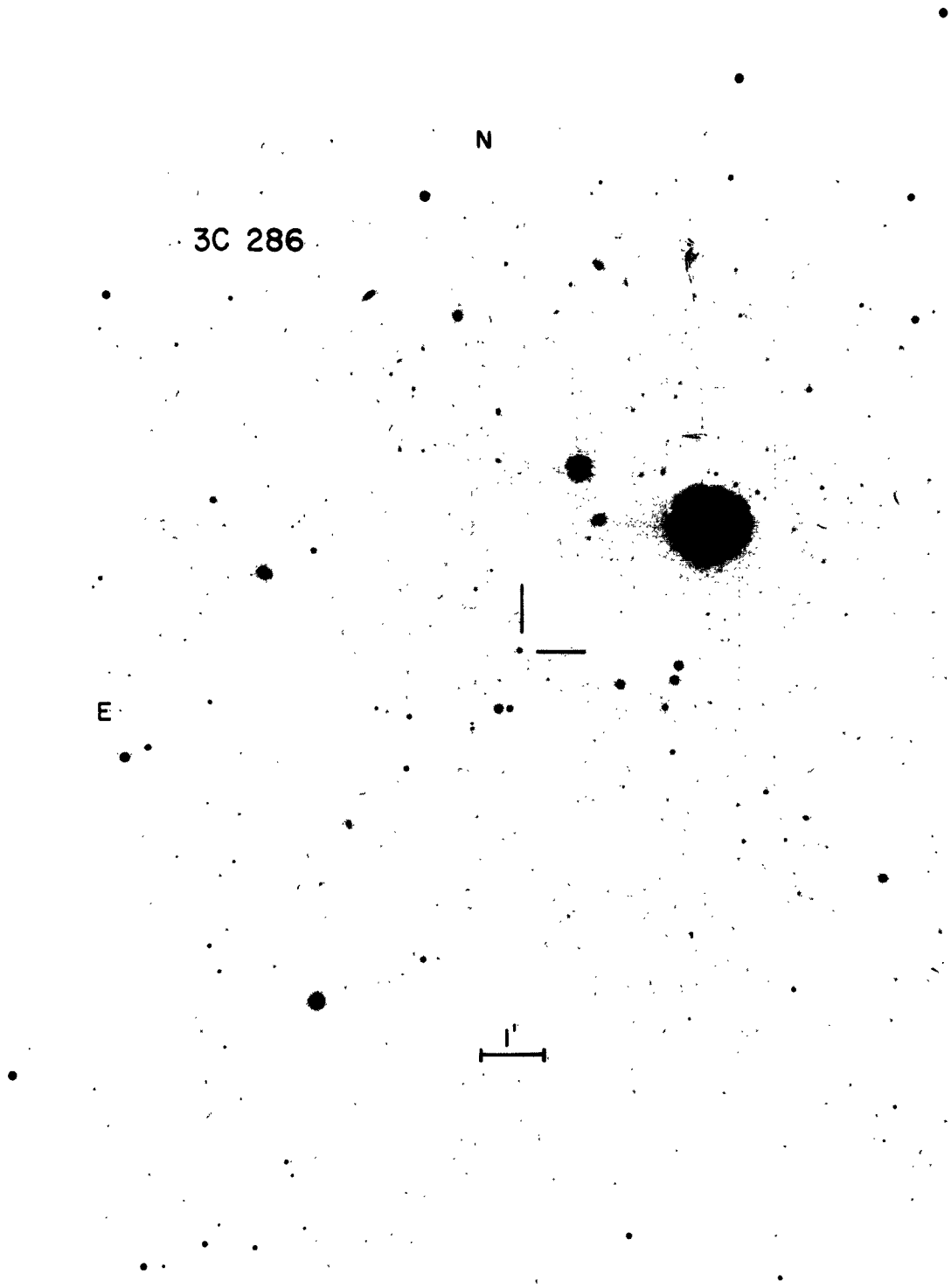

Figure 4. Finding chart for 3C 286.

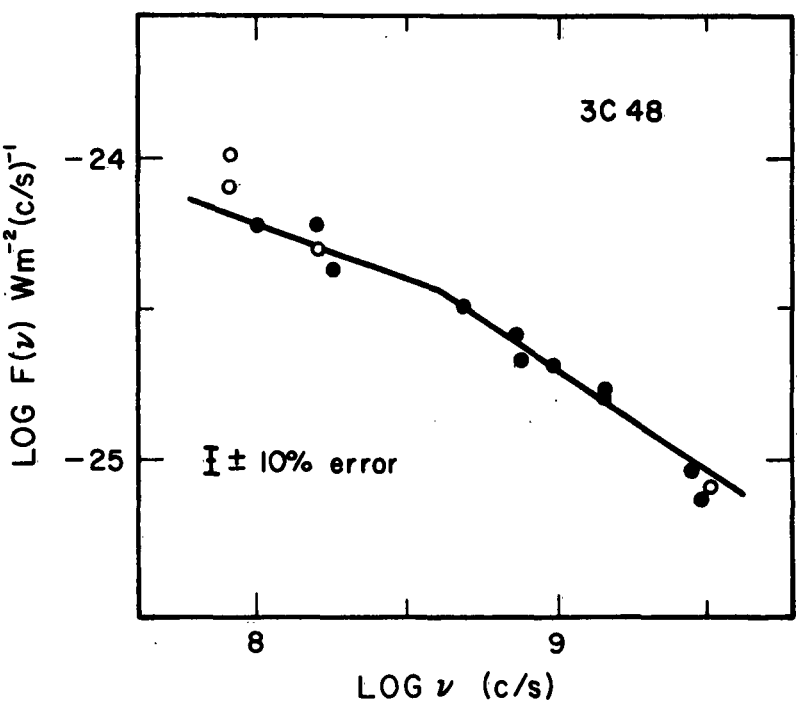

Figure 5. The radio power spectrum of 3C 48 taken from Table 3. The two straight lines have slopes of -0.67 and -0.47. The slope of -0.67 is that required in Figure 8 to fit the optical data.

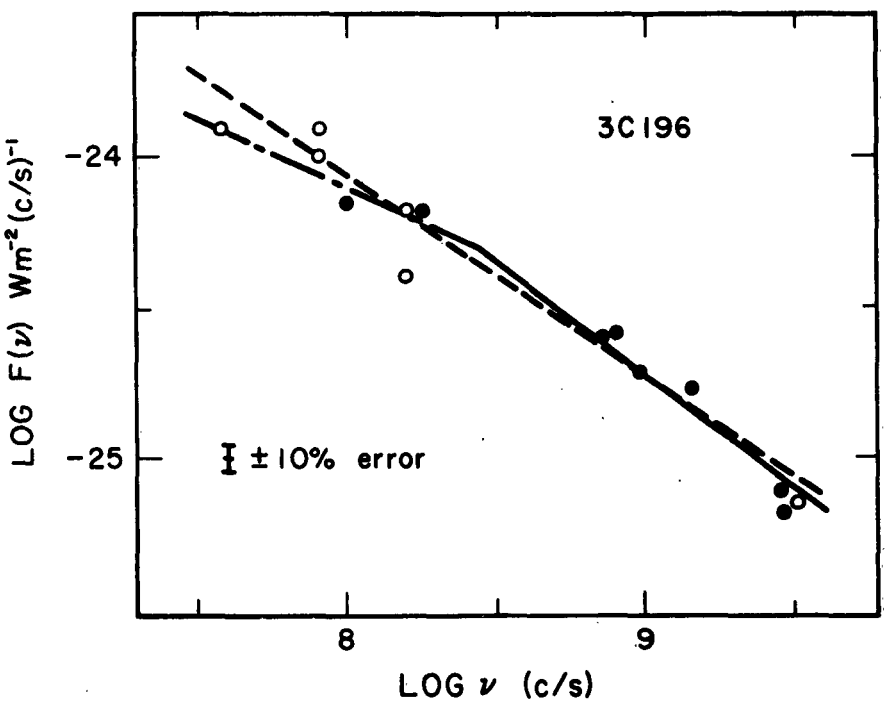

Figure 6. The radio power spectrum for 3C 196 taken from Table 4. The dotted line has a slope of -0.67 and gives the best representation of the radio data over the entire range. The solid line for $\nu > 4 \times 10^8$ c/s has a slope of -0.74 as required in Figure 10 to fit the optical data.

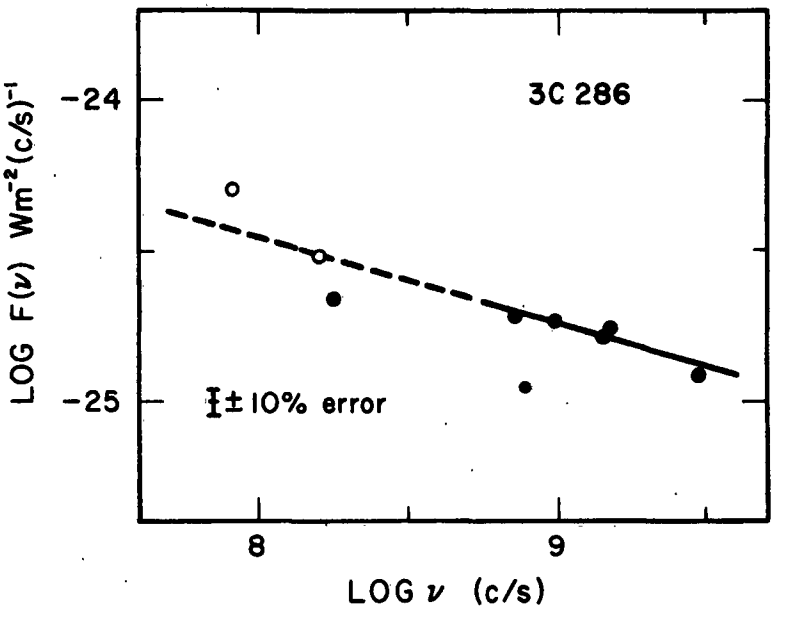

Figure 7. The radio power spectrum for 3C 286 taken from Table 5. The line has a slope of -0.28.

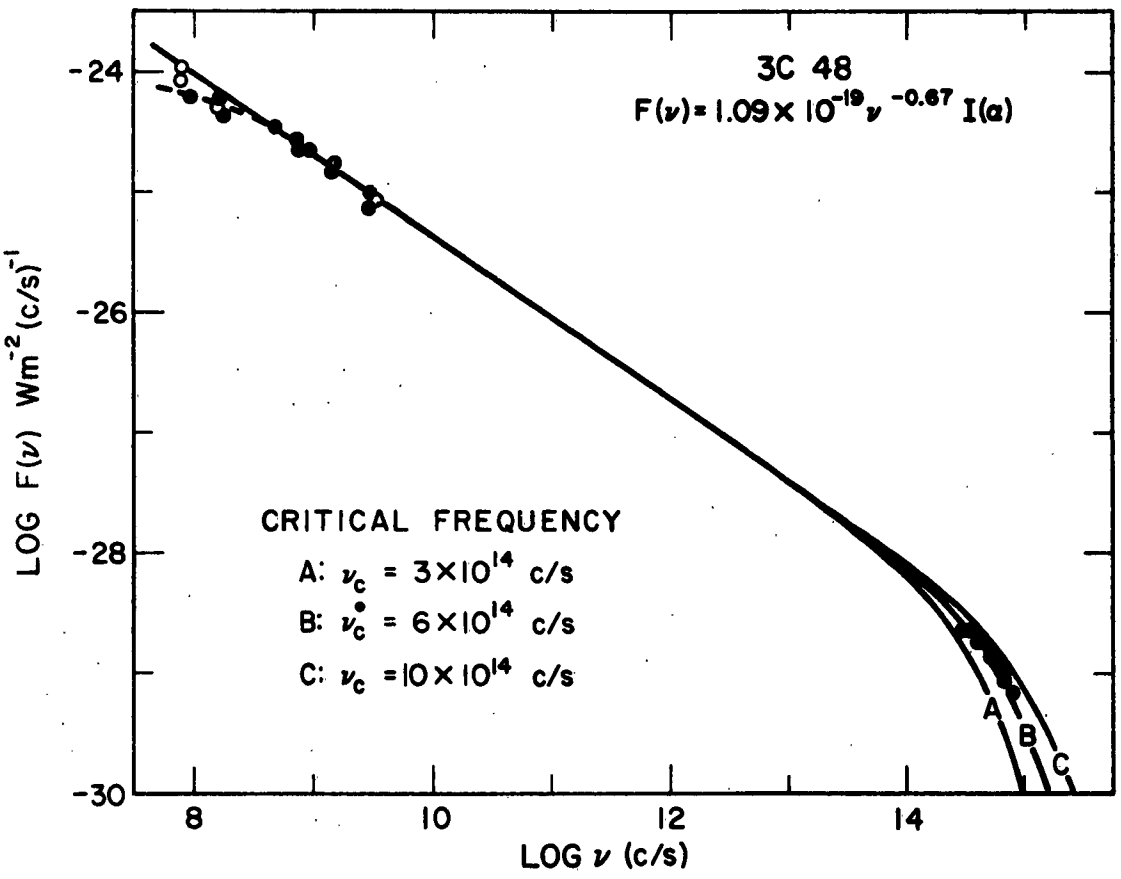

Figure 8. Comparison of the radio and optical power levels for 3C 48 with the theory of equation (5). The optical data are from Table 6.

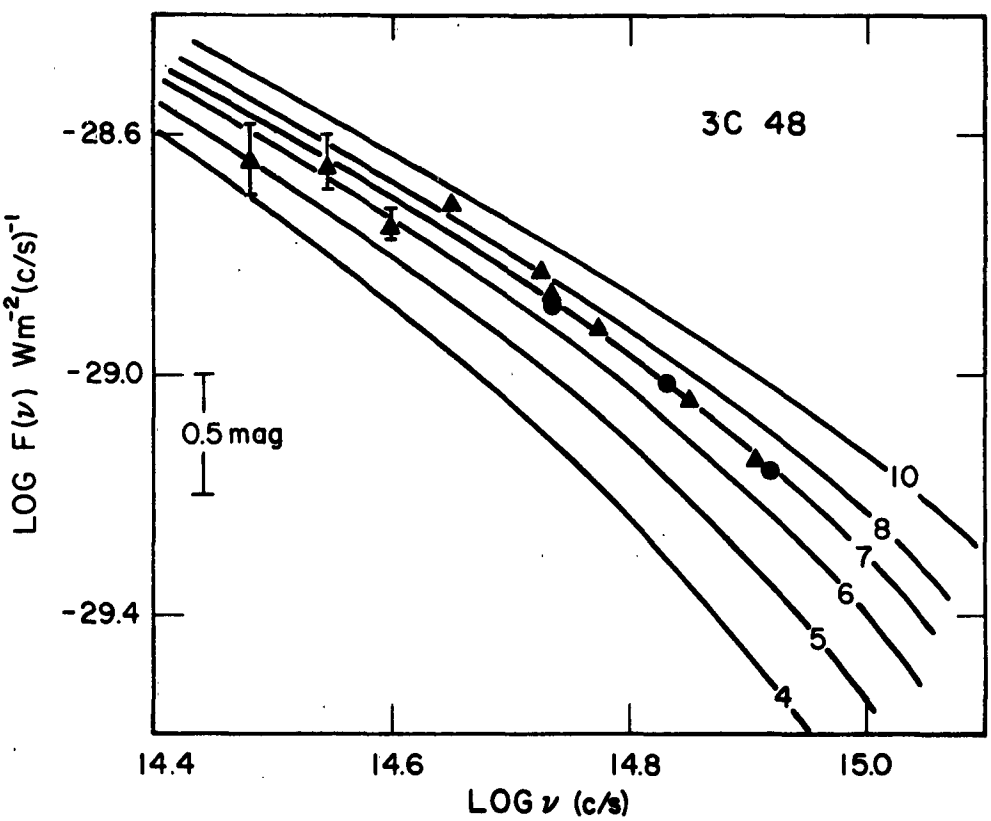

Figure 9. Detailed plot of the optical data for 3C 48 (Table 6) compared with the theoretical curves from equation (5) for various cut-off frequencies. The critical frequencies at the high energy cut-off are given on the curves in units of 10^{14} c/s.

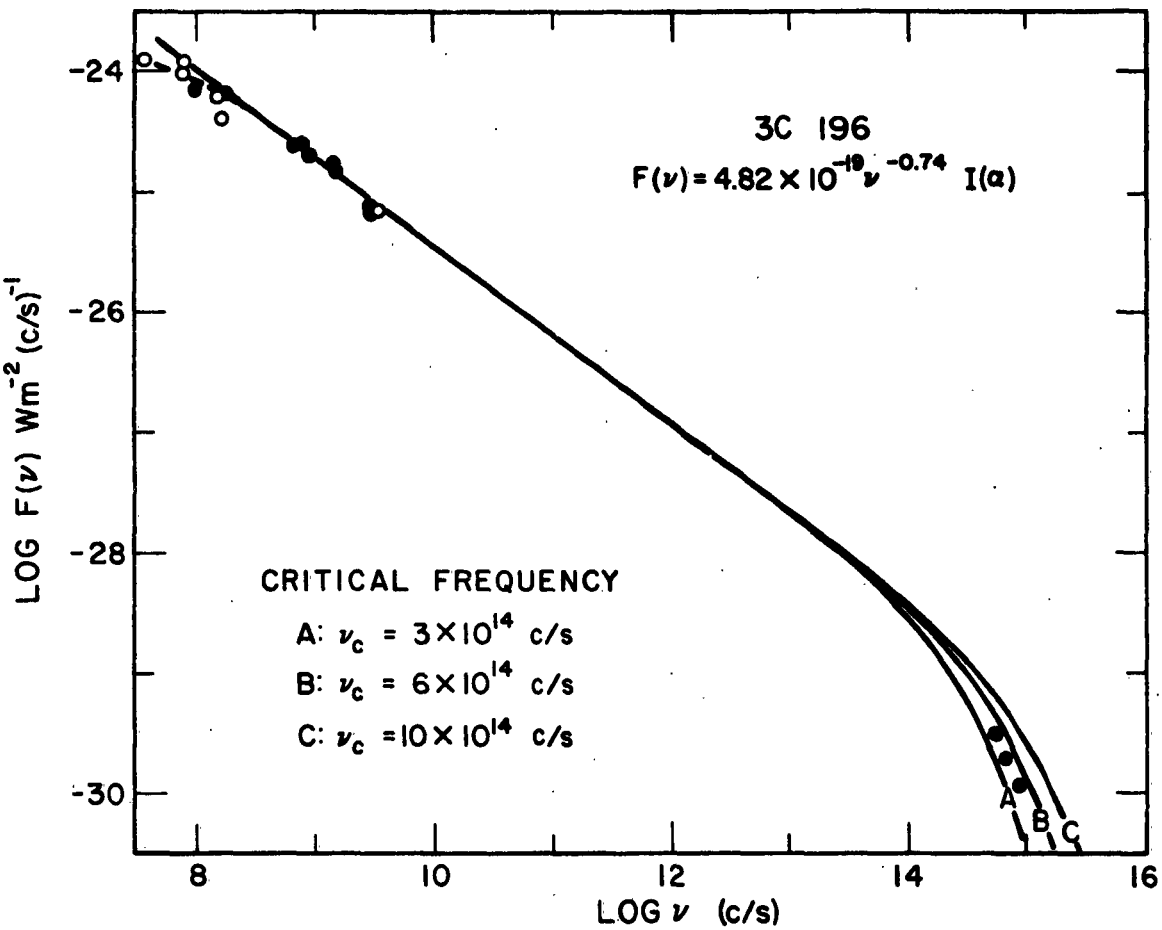

Figure 10. Comparison of the radio and optical power levels for 3C 196 with the theory of equation (5). The optical data are from Table 6.

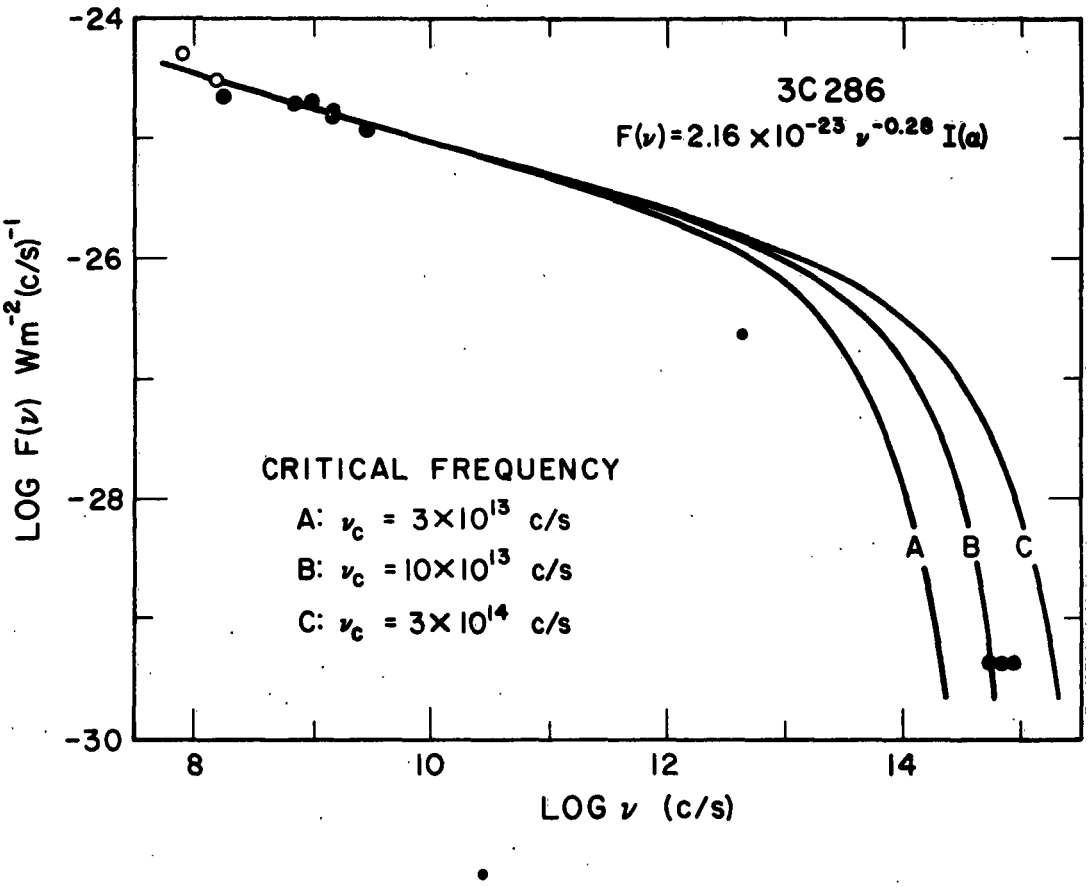

Figure 11. Comparison of the radio and optical power levels for 3C 286 with the theory of equation (5). The optical data are from Table 6.

Table 1

Photometric Data for the Three Radio Stars

Object	Date	V	B-V	U-B	Remarks
3C 48	Oct. 23/24, 1960	16.06	0.38	-0.61	
	Nov. 19/20, 1960	16.02	0.48	-0.61	60 inch
	Jan. 12/13, 1961	16.11	0.42	-0.61	
	Jan. 13/14, 1961	16.13	0.39	-0.61	
	Jan. 14/15, 1961	16.02	0.49	-0.60	
	Jan. 16/17, 1961	16.13	0.40	-0.59	
	Aug. 17/18, 1961	16.31	0.40	-0.52	
	Oct. 11/12, 1961	16.333	0.340	-0.579	Taken 15 min-
	Oct. 11/12, 1961	16.289	0.393	-0.555	utes apart
	Dec. 4/5, 1961	16.44	0.35	-0.57	Obs. by Baum
	Dec. 5/6, 1961	16.40	0.42	-0.64	Obs. by Baum
3C 196	Mar. 31/1, 1962	17.79	0.57	-0.43	
3C 286	June 2/3, 1962	17.25	0.26	-0.91	

Table 2

Radio and Optical Positions for Three Radio Stars

Source	α(1950.0)	ϵ_α	δ(1950.0)	ϵ_δ	Remarks
3C 48	$01^h34^m50^s.3$	$0^s.6$	$+32^\circ54'20''$	$2''$	Radio
	01 34 49.82	0.04	+32 54 20.2	0.5	Optical
3C 196	08 09 59.6	0.4	+48 22 06	2.6	Radio
	08 09 59.41	0.05	+48 22 07.9	0.5	Optical
3C 286	13 28 50.8	0.4	+30 45 55	6.5	Radio
	13 28 50.74	0.04	+30 45 59.5	0.5	Optical

Table 3

Radio Flux Measurements for 3C 48

Observer	ν (Mc/s)	$F(\nu)^*$	ϵ_p(%)	References
RSE 01.01	81	80	--	1
2C 133	81	102	--	2
BSS 92	100	60	20	3
3C	159	50	22	4
HBH	159	60	--	5
ERL	178	43	10	6
CIT(K)	475	33	6	7
CIT(K)	710	26.0	2	7
Heeschen	750	21.6	10	8
CIT(MM)	958	20.4	5	9,10
CIT(K)	1420	16.1	2	7
Goldstein	1423	17	5	11
CIT(B)	2841	9.2	5	12
Heeschen	3000	7.4	9	8
CIT(K)	3200	8.1	11	7

* The flux unit is 10^{-26} W $m^{-2}(c/s)^{-1}$.
The references are given at the bottom of Table 5.

Table 4

Radio Flux Measurements for 3C 196

Observer	ν (Mc/s)	$F(\nu)^*$	ϵ_p(%)	Ref.†	Remarks
Whitfield	38	125	56	13	Confused record
RSE 08.01	81	100	--	1	
2C 724	81	124	--	2	
BSS 84	100	70	20	3	
3C	159	66	30	4	
HBH	159	40	50	14	
ERL	178	66	10	6	
CIT(K)	710	25.2	1.2	7	
Heeschen	750	25.7	10	8	
CIT(MM)	958	19.4	4	9,10	
CIT(K)	1420	14.9	3	7	
Goldstein	1423	17	8	11	
CIT(B)	2841	7.5	5	12	
Heeschen	3000	6.7	10	8	
CIT(K)	3200	7.1	20	7	

* The flux unit is 10^{-26} W $m^{-2}(c/s)^{-1}$.
† The references are given at the bottom of Table 5.

Table 5

Radio Flux Measurements for 3C 286

Observer	ν(Mc/s)	$F(\nu)^*$	ϵ_p(%)	References
2C 1120	81	50	--	2
3C	159	30	23	4
ERL	178	22	10	6
CIT(K)	710	19.1	5	7
CIT(MM)	958	18.8	7	9,10
CIT(K)	1420	16	25	7
Goldstein	1423	17	6	11
CIT(B)	2841	12	6	12

* The flux unit is 10^{-26} W $m^{-2}(c/s)^{-1}$

References for Tables 3, 4, and 5

1. Ryle, M., Smith, F. G., and Elsmore, B. 1950, M.N., 110, 508.
2. Shakeshaft, J. R., Ryle, M., Baldwin, J. E., Elsmore, B., and Thomson, J. H. 1955, Mem. R. A. S., 67, 106.
3. Bolton, J. G., Stanley, G. J., and Slee, O. B. 1954, Australian J. Phys., 7, 110.
4. Edge, D. O., Shakeshaft, J. R., McAdam, W. B., Baldwin, J. E., and Archer, S. 1960, Mem. R. A. S., 68, 37.
5. Brown, R. H. and Hazard, C. 1959, M. N., 119, 297.
6. Elsmore, B., Ryle, M., and Leslie, P. R. R. 1960, Mem. R. A. S., 68, 61.
7. Kellermann, K. I., private communication.
8. Heeschen, D. S. and Meredith, B. L. 1961, Pub. Nat. Radio Astr. Obs., 1, 121.
9. Moffet, A. T., Ap. J. Suppl., 67. (in press).
10. Maltby, P., Ap. J. Suppl., 67. (in press).
11. Goldstein, S. J., 1962, A. J., 67, 171.
12. Bartlett, J. F., private communication.
13. Whitfield, G. R. 1960, M. N., 120, 581.
14. Brown, R. H. and Hazard, C. 1953, M. N., 113, 123.

Table 6

Optical Flux for the Three Radio Stars

Object	$\nu \times 10^{-14}$ c/s	$F(\nu)^*$	ϵ_F (%)	Remarks
3C 48	8.32	.669	1	U = 16.01
	6.77	.958	1	B = 16.60
	5.42	1.29	1	V = 16.20
	8.07	.718	1	Baum Eight Color Data Reduced to V = 16.20
	7.09	.900	1	
	5.94	1.19	1	
	5.46	1.35	1	
	5.31	1.46	1	
	4.50	1.94	3	
	3.99	1.78	4	
	3.53	2.24	12	
	3.04	2.26	14	
3C 196	8.32	.124	2	U = 17.93
	6.77	.195	2	B = 18.36
	5.41	.302	2	V = 17.79
3C 286	8.35	.421	2	U = 16.60
	6.81	.416	2	B = 17.51
	5.44	.403	2	V = 17.25

* The units for $F(\nu)$ are 10^{-29} W $m^{-2}(c/s)^{-1}$.

TABLE 7

Physical Parameters at an Assumed Distance of One Parsec

Source	$M_V(1)$	V(1) (cm^3)	$\nu_2 = 10^{10}$ c/s				ν_2*			
			L(1) $\left(\frac{erg}{sec}\right)$	H(1) (gauss)	$E_T(1)$ (erg)	$\tau(1)$ (year)	L(1) $\left(\frac{erg}{sec}\right)$	H(1) (gauss)	$E_T(1)$ (erg)	$\tau(1)$ (year)
3C 48	21									
Core S = 1″		1.8×10^{39}	1.39×10^{26}	0.20	1.2×10^{37}	12	6.18×10^{27}	0.22	1.5×10^{37}	0.33
S = 0.″1		1.8×10^{36}	1.39×10^{26}	1.4	6.4×10^{35}	0.62	6.18×10^{27}	1.6	7.8×10^{35}	0.017
3C 196	23									
Halo		3.0×10^{42}	9.89×10^{25}	0.022	2.7×10^{38}	370	2.04×10^{27}	0.041	9.2×10^{38}	61
Core S = 1″		1.8×10^{39}	3.30×10^{25}	0.14	5.9×10^{36}	24	6.82×10^{26}	0.25	2.0×10^{37}	4.8
S = 0.″1		1.8×10^{36}	3.30×10^{25}	0.99	3.1×10^{35}	1.2	6.82×10^{26}	1.8	1.0×10^{36}	0.25
3C 286	22									
Halo		1.4×10^{43}	6.28×10^{25}	0.010	2.6×10^{38}	550	9.70×10^{27}	0.017	7.2×10^{38}	9.9
Core S = 1″		1.8×10^{39}	9.42×10^{25}	0.15	6.9×10^{36}	9.9	1.46×10^{28}	0.25	1.9×10^{37}	9.18
S = 0.″1		1.8×10^{36}	9.42×10^{25}	1.1	3.6×10^{35}	0.51	1.46×10^{28}	1.8	1.0×10^{36}	0.0092

*The upper cut-off frequencies used are:

3C 48 $\nu_2 = 7\times10^{14}$ c/s

3C 196 $\nu_2 = 4\times10^{14}$ c/s

3C 286 $\nu_2 = 10\times10^{12}$ c/s

Table 8

Scaling Factors for Other Distances

r(pcs)	$M_V - M_V(1)$	$\frac{V(r)}{V(1)}$	$\frac{L(r)}{L(1)}$	$\frac{H(r)}{H(1)}$	$\frac{E_T(r)}{E_T(1)}$	$\frac{\tau(r)}{\tau(1)}$
1	0	1	1	1	1	1
10	-5	10^3	10^2	0.52	2.7×10^2	2.7
10^2	-10	10^6	10^4	0.27	7.2×10^4	7.2
10^3	-15	10^9	10^6	0.14	2.0×10^7	20
10^4	-20	10^{12}	10^8	0.072	5.2×10^9	52
10^5	-25	10^{15}	10^{10}	0.037	1.4×10^{12}	140

Table 9

Average Values of Physical Parameters at 100 pcs

	V (cm^3)	H (gauss)	E_T (erg)	$\nu_2 = 10^{10}$ c/s		$\nu_2 \approx 10^{14}$ c/s	
				L (erg sec^{-1})	τ (year)	L (erg sec^{-1})	τ (year)
Halo	10^{49}	5×10^{-3}	4×10^{43}	8×10^{29}	3000	6×10^{31}	200
Core S=1"	2×10^{42}	5×10^{-2}	7×10^{41}	9×10^{29}	100	5×10^{31}	15
S=0".1	2×10^{39}	4×10^{-1}	4×10^{40}	9×10^{29}	5	5×10^{31}	0.5

APPENDIX A

Theoretical U-B, B-V Colors for Spectral Distributions of Arbitrary Form

In many applications it is desirable to compute the colors on the U, B, V system of radiant sources with given energy distributions. This can be done once the transmission functions $S(\lambda)$ of the U, B, V system are known. Melbourne showed (1960) that the $S(\lambda)$ functions tabulated by H. L. Johnson (1955) as representing the system will not predict exactly the observed U-B, B-V colors for real stars of known energy distributions unless a systematic zero point correction of $0^m.17$ is added to the computed natural u-b magnitude and a correction of -0.13 is applied to the computed natural b-v magnitude before applying Johnson's empirically determined transformation equation (5) of Ap. J. 117, 313, 1953. These corrections assume that there is no color equation between the theoretical colors based on $S(\lambda)$ and the U-B and B-V values adopted for standard stars in the sky. In this appendix we confirm Melbourne's zero point procedure for B-V colors by showing that his adopted $S(\lambda)$ functions predict the natural colors $(b-v)_o$ outside the atmosphere for seven real stars such that the regression line of $(b-v)_o$ on the known B-V colors has a slope of 1.00. However, this is not the case in U-B where the adopted $S(\lambda)$ functions predict $(u-b)_o$ colors with a longer baseline than the observed U-B; i.e. a color equation exists. The equations derived in this appendix can be used to convert theoretical calculations based on the adopted $S(\lambda)$ to the empirical U, B, V system. Predicted U-B, B-V colors for <u>any</u> arbitrary flux distribution function $F(\lambda)$ can be obtained therefrom.

Table A1, taken from Melbourne's thesis, lists the transmission functions for the theoretical photometric system designated by u, b, v. As anticipated in the last paragraph, this system, aside from zero point corrections, is close to, but not identical with, U, B, V. The $S(\lambda)$ functions were constructed by A. D. Code from Johnson's tabulated values for zero air mass by applying the monochromatic extinction of the atmosphere for one and two air masses as determined from spectrum scanner observations (Code, as tabulated by Melbourne 1960, Table 2). We have tabulated these functions because they are needed in what follows and they appear nowhere in the literature. The $S(\lambda)$ for one air mass was tabulated by Arp (1961) in his discussion of U-B, B-V colors for black bodies, but $S(\lambda)_o$ and $S(\lambda)_2$ are needed for a full treatment of the problem.

The $S(\lambda)_1$, and $S(\lambda)_2$ functions of Table A1 were used to operate on the relative energy distributions $F(\lambda)$ for seven real stars. The $F(\lambda)$ data were obtained from Minnaert (1953, Table 1), Code (1960) and Melbourne (1960). Code and Melbourne tabulate 2.5 log $F(\nu)$ where $F(\nu)$ is the energy flux per unit frequency interval. The $F(\nu)$ values were converted to relative energy flux per wavelength interval $F(\lambda)$ by multiplying $F(\nu)$ by λ^{-2}. The seven stars chosen were either relatively free from Fraunhofer lines or, as in the case of the sun (Minnaert 1953, Table 1), the continuum level was already adjusted to compensate for the effect of the lines.

Theoretical colors on the natural system of $S(\lambda)$ for one and two air masses were computed from

$$(u-b)_i = 2.5 \log \frac{\int_0^\infty S_b(\lambda)_i \, F(\lambda) \, d\lambda}{\int_0^\infty S_u(\lambda)_i \, F(\lambda) \, d\lambda} \, , \; i = 1 \text{ or } 2, \qquad \text{(A1)}$$

with a similar equation for $(b-v)_1$ and $(b-v)_2$. In an obvious notation the subscripts refer to 1 or 2 air masses. Results for the seven stars are listed in Table A2 where the observed U-B, B-V colors are shown in columns 2 and 3, the computed natural colors $(b-v)_1$, $(b-v)_2$ in columns 4 and 5, $(u-b)_1$, $(u-b)_2$ in columns 6 and 7, and the differences $k_{12} \equiv (b-v)_2-(b-v)_1$ and $k_{56} \equiv (u-b)_2-(u-b)_1$ in columns 8 and 9. Note that k_{12} and k_{56} represent the color extinction between sec Z = 2 and sec Z = 1 and therefore are related to the usual extinction coefficients defined by

$$k_{12} \equiv k_1-k_2 \, (b-v)_o \qquad \text{(A2)}$$

$$k_{56} \equiv k_5-k_6 \, (u-b)_o \, . \qquad \text{(A3)}$$

As was expected, the extinction coefficients k_{12} and k_{56} are color dependent according to our calculations (i.e. k_2 and k_6 are not zero). From Table A2 it is easily shown that

$$k_{12} = 0.102-0.024 \, (b-v)_o \qquad \text{(A4)}$$

which is in excellent agreement with observational determinations of extinction on good nights over the past 10 years on Mount Wilson. The extinction coefficient k_{56} cannot be represented by such a simple equation over the range of $(u-b)_o$ covered by our seven calibrating stars. The value of k_6 depends on $(u-b)_o$ itself, which shows that equation (A3) does not represent the broad band ultraviolet-blue extinction. The variation of k_6 with $(u-b)_o$ has been found observationally (Johnson, unpublished communication). It should be emphasized that in setting up the U-B system in 1953, Johnson intentionally put $k_6 = 0$ to avoid the great complication involved in the reduction procedure of $k_6 = f[(u-b)_o]$. Therefore, if we are to compare theoretically computed u-b indices with U-B values assigned to real stars, we must ignore the color variation of k_{56} even though $k_6 \neq 0$ in nature. The adopted U-B values for stars in the sky therefore contain slight inconsistencies with a purely theoretical system. Consequently, in the following we shall relate the computed $(u-b)_1$ values directly to U-B rather than use the theoretical k_{56} value from Table A2 to obtain $(u-b)_o$ from $(u-b)_1$ in the usual way [i.e. $(u-b)_o = (u-b)_1 - k_{56}$] and then to find $(u-b)_o = f(U-B)$. We tried this latter procedure, which is theoretically correct because it takes the non-zero k_6 term into account, but the correlation of $(u-b)_o$ and U-B was non-linear, deviating by $\pm 0^m.05$ from straight line. The foregoing explanation is believed to be correct (i.e. small, residual inconsistencies in the actual U-B values), because the non-linearity was eliminated in a plot of $(u-b)_1$ vs U-B. Conversations with Harold Johnson after these calculations were completed confirm that this is undoubtedly the case.

With the foregoing precepts and with the data of Table A2, the following extinction and color equations can be derived. From equation (A4) and from the definition of extinction coefficients, which is

$$(b-v)_o = (b-v)_{\sec Z} - \left[k_1 - k_2 (b-v)_o\right] \sec Z, \qquad (A5)$$

it follows that

$$(b-v)_o = 1.024\ (b-v)_1 - 0.104\ . \qquad (A6)$$

With $(b-v)_o$ now known by using equation (A6) and the $(b-v)_1$ values of Table A2, we correlate $(b-v)_o$ with the observed B-V for the seven calibrating stars. The result is

$$B-V = 1.00\ (b-v)_o + 0.91 \qquad (A7)$$

or

$$B-V = 1.024(b-v)_1 + 0.81 \qquad (A8)$$

which shows that there is no color equation between Table A1 and the B-V system if the extinction is treated in this way.

The U-B situation is different. No extinction values were applied to $(u-b)_1$ to obtain $(u-b)_o$ for the reasons previously discussed. Direct comparison of $(u-b)_1$ and U-B from Table A2 gives the well determined relation

$$U-B = 0.921\ (u-b)_1 - 1.308 \qquad (A9)$$

which is the color equation between the <u>observed</u> U-B system and the <u>theoretical</u> $(u-b)_1$ system.

An objection might be raised to our procedure in that, in actual fact, we may not know the true $F(\lambda)$ for the seven calibrating stars of Table A2 due to the effects of line blanketing, with the result that our predicted $(u-b)_1$ colors may be in error. While this objection may be true for σ Boo, and to a lesser extent for α Lyrae with its strong hydrogen lines, it is not true for the other stars. 10 Lac and η UMa are so hot as to have few lines; HD 19445 and HD 140283 are cool subdwarfs with extremely weak Fraunhofer lines and the blanketing effect is almost nil, while the effect in the sun has been corrected for by Minnaert before giving his $F(\lambda)$ of his Table 1 (1953). Therefore we interpret the slope coefficient in equation (A9) to differ significantly from 1.00 and suggest that a color equation exists. We are not completely confident of the result because of the blanketing problem, but accept it for the present.

Equations (A8) and (A9) solve the problem. To compute U-B and B-V for any arbitrary energy distribution $F(\lambda)$, proceed as follows. (1) Use the $S(\lambda)_1$ functions of Table A1 and use equation (A1) to compute natural colors $(u-b)_1$ and $(b-v)_1$. (2) Use equations (A8) and (A9) to find U-B and B-V. A check on the internal consistency of this procedure is made by applying the equations to the seven calibrating stars. Comparison of the computed colors in columns (10) and (11) of Table A2 with the observed colors of columns (2) and (3) shows good agreement.

The above procedure differs from that used by Arp (1961) in that we have used a color equation (A9) to the U-B system whereas Arp had none. Our zero points also differ slightly. Table A3 shows the difference between Arp's calculations of the black body line and our own. The difference is very small.

In the theory of synchrotron radiation, energy distributions of the form $F(\nu) \propto \nu^{-n}$ (flux per unit frequency interval) are found. Calculation of U-B and B-V values have been made for these distributions for various values of n ranging from 0.0 to 2.0 in steps of 0.2. The sources were assumed to radiate as $F(\lambda) \propto \lambda^{n-2}$ (per unit wave length interval). The results are given in Table A4 and have been discussed in the body of the paper.

TABLE A1

Adopted Transmission Functions After Melbourne and Code

$\lambda \times 10^{-2}$ Å	$S(\lambda)_0$		$S(\lambda)_1$, One Air Mass			$S(\lambda)_2$, Two Air Masses		
	b_0	v_0	u_1	b_1	v_1	u_2	b_2	v_2
30			0.025			0.025		
31			0.250			0.060		
32			0.680			0.170		
33			1.137			0.375		
34			1.650			0.675		
35	0.000		2.006	0.000		1.000		
36	0.015		2.250	0.006		1.250	0.000	
37	0.100		2.337	0.080		1.390	0.040	
38	0.500		1.925	0.337		1.125	0.250	
39	1.800		0.650	1.425		0.600	0.870	
40	3.620		0.197	2.253		0.140	1.745	
41	3.910		0.070	2.806		0.030	2.025	
42	4.000		0.000	2.950		0.000	2.200	
43	3.980			3.000			2.290	
44	3.780			2.937			2.290	
45	3.500			2.780			2.200	
46	3.150			2.520			2.050	
47	2.700	0.000		2.230			1.840	0.000
48	2.320	0.020		1.881	0.020		1.580	0.020
49	1.890	0.280		1.550	0.175		1.325	0.175
50	1.530	1.180		1.275	0.900		1.079	0.830
51	1.140	2.170		0.975	1.880		0.840	1.570
52	0.750	2.970		0.695	2.512		0.580	2.150
53	0.500	3.300		0.430	2.850		0.360	2.420
54	0.250	3.250		0.210	2.820		0.180	2.425
55	0.070	3.000		0.055	2.625		0.050	2.270
56	0.000	2.700		0.000	2.370		0.000	2.035
57		2.320			2.050			1.780
58		2.000			1.720			1.530
59		1.670			1.413			1.255
60		1.280			1.068			0.985
61		0.920			0.795			0.745
62		0.650			0.567			0.505
63		0.430			0.387			0.340
64		0.260			0.250			0.220
65		0.175			0.160			0.140
66		0.125			0.110			0.100
67		0.100			0.081			0.080
68		0.070			0.061			0.055
69		0.050			0.045			0.030
70		0.030			0.028			0.025
71		0.020			0.017			0.010
72		0.010			0.007			0.000

Tabulated are the transmissions of two aluminum reflections, filters, 1P21 photomultiplier, and atmosphere for zero, one, and two air masses.

Table A2

Computed and Observed Colors for the Seven Calibrating Stars

(1)	(2)	(3)	(4)	(5)	(6)	(7)	(8)	(9)	(10)	(11)
Star	$(B-V)_{obs}$	$(U-B)_{obs}$	$(b-v)_1$	$(b-v)_2$	$(u-b)_1$	$(u-b)_2$	k_{12}	k_{56}	$(B-V)_c$	$(U-B)_c$
10 Lac	-0.20	-1.04	-0.994	-0.864	0.284	0.743	0.130	0.459	-0.21	-1.05
η U Ma	-0.21	-0.68	-0.984	-0.857	0.683	1.121	0.127	0.438	-0.20	-0.68
HD 19445	0.46	-0.24	-0.338	-0.223	1.182	1.596	0.115	0.414	0.46	-0.22
HD 140283	0.48	-0.20	-0.288	-0.174	1.161	1.567	0.114	0.406	0.51	-0.24
σ Boo	0.37	-0.09	-0.436	-0.320	1.332	1.725	0.116	0.393	0.36	-0.08
α Lyr	0.00	-0.01	-0.839	-0.714	1.410	1.762	0.125	0.352	-0.05	-0.01
Sun	0.62	0.10	-0.196	-0.090	1.512	1.933	0.106	0.421	0.61	0.08

Table A3

Black Body Line in the U-B, B-V Diagram

	Present		Arp	
T_e	U-B	B-V	$(U-B)_A$	$(B-V)_A$
∞	-1.28	-0.44	-1.33	-0.46
25,000	-1.13	-0.21	-1.17	-0.23
20,000	-1.06	-0.15	-1.09	-0.17
12,000	-0.83	+0.05	-0.84	+0.04
8,000	-0.53	+0.35	-0.52	+0.34
6,000	-0.26	+0.63	-0.22	+0.61
5,000	-0.10	+0.79	-0.05	+0.78
4,000	+0.36	+1.13	+0.37	+1.12
3,300	+0.78	+1.44	+0.83	+1.44
3,000	+1.07	+1.67	+1.14	+1.66

Table A4

U-B, B-V Colors for Sources with $F(\nu) = C\,\nu^{-n}$

n	$(u-b)_1$	$(b-v)_1$	U-B	B-V
0.0	0.440	-0.697	-0.90	0.10
0.2	0.487	-0.648	-0.86	0.15
0.4	0.534	-0.600	-0.82	0.20
0.6	0.582	-0.551	-0.77	0.25
0.8	0.629	-0.503	-0.73	0.30
1.0	0.677	-0.454	-0.68	0.34
1.2	0.724	-0.406	-0.64	0.39
1.4	0.772	-0.358	-0.60	0.44
1.6	0.820	-0.310	-0.55	0.49
1.8	0.868	-0.263	-0.51	0.54
2.0	0.916	-0.215	-0.46	0.58

APPENDIX B

Conversion of UBV Optical Data to Absolute Flux Units

The most recent calibration of the energy flux in absolute units arriving from a star of apparent visual magnitude V = 0 is due to Willstrop (1960). We adopt Willstrop's Table 1 for the energy flux per Å at λ5390 for stars of V = 0.00, and take the known relative energy distribution curves for stars of different B-V values to compute the absolute flux calibrations at the effective wavelengths of the U, B, and V points for stars of U = B = V = 0.

a) Effective Wavelengths for the UBV Filters

The effective wavelength of any filter system depends upon the energy distribution F(λ) of the source which is measured with the system. We define the effective wavelength in the usual way by

$$\bar{\lambda} = \frac{\int_0^\infty \lambda S(\lambda)\ F(\lambda)\ d\lambda}{\int_0^\infty S(\lambda)\ F(\lambda)\ d\lambda} \qquad \text{(B1)}$$

and compute $\bar{\lambda}$ for sources characterized by $F(\lambda) \propto \lambda^{n-2}$.

The effective wavelengths calculated from equation (B1) using the S(λ) function from Table A1 are for the u, b, v natural system, which is related to the UBV system via equations (A7), (A8), and (A9) of Appendix A. From these equations and from $\bar{\lambda}_u$, $\bar{\lambda}_b$, $\bar{\lambda}_v$ for one air mass, we can obtain $\bar{\lambda}_U$, $\bar{\lambda}_B$, $\bar{\lambda}_V$ for the actual UBV system as follows.

The relation between two color systems, characterized by effective wavelengths λ_1, λ_2, and λ_3, λ_4, when the measurements are made on black bodies is

$$\frac{(C.I.)_{1,2}}{(C.I.)_{3,4}} = \frac{\frac{1}{\lambda_1} - \frac{1}{\lambda_2}}{\frac{1}{\lambda_3} - \frac{1}{\lambda_4}} \qquad \text{(B2)}$$

For sources we are considering where $F(\lambda) \propto \lambda^{n-2}$, the correct relation will be

$$\frac{(C.I.)_{1,2}}{(C.I.)_{3,4}} = \frac{\log\left(\frac{1}{\lambda_1}\right) - \log\left(\frac{1}{\lambda_2}\right)}{\log\left(\frac{1}{\lambda_3}\right) - \log\left(\frac{1}{\lambda_4}\right)} \qquad \text{(B3)}$$

but for color systems where the effective wavelengths are very close to one another, equation (B2) and (B3) give nearly identical answers. We use equation (B2) in the following.

The effective wavelength of V was obtained by assuming $\bar{\lambda}_V \equiv \bar{\lambda}_v$ for $S_V(\lambda)_o$ in equation (B1). This gives $\bar{\lambda}_V$ listed in column 6 of Table B1 for various n values. The $\bar{\lambda}_B$ follows from equation (B2) and equation

(A8) as

$$\frac{1}{\bar{\lambda}_B} = \frac{1}{\bar{\lambda}_V} + 1.024\left[\frac{1}{\bar{\lambda}_{b_1}} - \frac{1}{\bar{\lambda}_{v_1}}\right] \qquad (B4)$$

where $\bar{\lambda}_{b1}$ is the effective wavelength of the natural b system for 1 air mass and likewise for v in $\bar{\lambda}_{v1}$. A check on the above procedure is available from equation (A7) which requires that $\bar{\lambda}_B = \bar{\lambda}_{b0}$. The check was made and was found to be excellent. Column 5 of Table B1 gives $\bar{\lambda}_B$.

For the ultraviolet, equation (A9) requires

$$\frac{1}{\bar{\lambda}_U} = \frac{1}{\bar{\lambda}_B} + 0.921\left[\frac{1}{\bar{\lambda}_{u1}} - \frac{1}{\bar{\lambda}_{b1}}\right] \qquad (B5)$$

where all quantities on the right side are now known or were computed from equation (B1). Column 4 of Table B1 gives $\bar{\lambda}_U$ for the various n values.

b) Calibration of Magnitudes in Absolute Flux Units

Willstrop, in his Table 1 (1960), gives absolute monochromatic fluxes at λ = 5390 Å, a wavelength which differs from $\bar{\lambda}_V$. We need the ratio $F(\bar{\lambda}_V)/F(5390)$ to correct Willstrop's values to monochromatic fluxes at $\bar{\lambda}_V$. For the sources we are considering, where $F(\lambda) = C\lambda^{n-2}$, it follows that

$$\log \frac{F(\bar{\lambda}_V)}{F(5390)} = (n-2)\log\left(\frac{\bar{\lambda}_V}{5390}\right) \qquad (B6)$$

From equation (B6), from Willstrop's Table 1, and from the conversion of flux units in ergs cm^{-2} sec^{-1} $Å^{-1}$ to W $m^{-2}(c/s)^{-1}$ by multiplying the former by 10^5 λ^2/c to get the latter, we obtain the flux at $\bar{\lambda}_V$ for a source of visual magnitude V = 0 tabulated in column 9 of Table B1, which is one of the three answers we require. The flux at the effective wavelengths of the B and U bands are now found as follows. For a given index n (for example n = 2), the flux in the source at the wavelengths $\bar{\lambda}_V$ and $\bar{\lambda}_B$ are in the ratio $(\nu_V/\nu_B)^{-2}$ = 1.5596 (for n = 2) per unit frequency interval. Thus, if the visual magnitude of the source were 0.00, the absolute flux density in W m^{-2} $(c/s)^{-1}$ at $\bar{\lambda}_B$ = 4440 Å would be 1.5596 times the flux at $\bar{\lambda}_V$ which we have previously calculated and listed in Table B1. But Table A4 or B1 show that B-V = +0.58 for n = 2, or B = +0.58 by the requirement that V = 0.00. Hence, the flux at $\bar{\lambda}_B$ = 4440 for a source of index n = 2 corresponding to a blue magnitude 0.00 will be 1.84×10^{-23} W m^{-2} $(c/s)^{-1}$. Similar calculations were made for all cases and are tabulated in Table B1 and these numbers solve the problem.

Table B1

Adopted Effective Wavelengths and Conversions to Absolute Flux Units for the U, B, V System for Sources which Radiate as $F(\nu) = C\nu^{-n}$

(1)	(2)	(3)	(4)	(5)	(6)	(7)	(8)	(9)
n	U-B	B-V	$\bar{\lambda}_U$	$\bar{\lambda}_B$	$\bar{\lambda}_V$	$F(\nu)_U$	$F(\nu)_B$	$F(\nu)_V$
0.0	-0.91	0.10	3585	4383	5502	1.79	4.13	3.81
0.2	-0.86	0.15	3586	4387	5505	1.80	4.15	3.82
0.6	-0.77	0.25	3593	4408	5515	1.81	4.18	3.84
1.0	-0.68	0.34	3598	4412	5525	1.82	4.21	3.87
1.4	-0.60	0.44	3604	4431	5534	1.83	4.26	3.90
2.0	-0.46	0.58	3610	4440	5545	1.84	4.31	3.94

U-B and B-V taken from Table A4 of Appendix A.
The unit on the flux is 10^{-23} W $m^{-2}(c/s)^{-1}$ for a star of U=B=V=0 apparent magnitude.

REFERENCES

Allen, L. R., Anderson, B., Conway, R. G., Palmer, H. P., Reddish, V.C., and Rowson, B. 1962, M.N. (in press).

Arp, H. C. 1961, Ap.J., 133, 874.

Bolton, J. G., Sept. 1960, U.R.S.I. General Assembly, London. Observations of California Institute Technology, 5.

Burbidge, G. R. 1956, Ap.J., 124, 416.

Burbidge, G. R. 1959, Paris Symposium on Radio Astronomy, ed. R. N. Bracewell (Stanford, Calif.: Stanford University Press), p. 541.

Burbidge, G. R. and Burbidge, E. M. 1957, Ap.J., 125, 1.

Code, A. D. 1960, Stellar Atmospheres, ed. J. L. Greenstein (Chicago: University of Chicago Press), Chap. 2.

Conway, R. G., Kellermann, K. I., and Long, R. J. 1962, M.N. (in press).

Edge, D. O., Shakeshaft, J. R., McAdam, W. B., Baldwin, J. E. and Archer, S. 1959, Mem.R.A.S., 68, 37.

Greenstein, J. L. 1958, Handbuch der Physik, 50, ed. S. Flugge (Berlin: Springer) p. 161.

Johnson, H. L. 1955, Ann. d'Ap., 18, 292.

Kellermann, K. I., Long, R. J., Allen, L. R., and Moran, M. 1962, Nature, 195, 692.

Maltby, P. and Moffet, A. T. 1962, Ap.J.Suppl., 67.

Maltby, P., Matthews, T. A., and Moffet, A. T. 1963, Ap.J. (in press).

Matthews, T. A., Bolton, J. G., Greenstein, J. L., Münch, G., and Sandage, A. R. 1961, Sky and Telescope, 21, 148.

Melbourne, W. G. 1960, Ap.J., 132, 101.

Minnaert, M. 1953, The Sun, ed. G. P. Kuiper (Chicago: University of Chicago Press) Chap. 3.

Oort, J. H. and Walraven, T. 1956, B.A.N., 12, 285.

Payne-Gaposchkin, C. 1957, The Galactic Novae (Amsterdam: North Holland Publishing Co.).

Read, R. B. 1962, Ph.D.Thesis (unpublished), Calif. Inst. of Tech.

Rowson, B. 1962, submitted to M.N.

Ryle, M. and Clarke, R. W. 1961, M.N., 122, 349.

Schmidt, M. 1962a, Ap.J., 136, 684.

Schmidt, M. 1962b, Ap.J., (in press).

Schwinger, J. 1949, Phys. Rev., 75, 1912.

Scott, P. F., Ryle, M., and Hewish, A. 1961, M.N., 122, 95.

References (continued)

Smith, H. J. and Hoffleit, D. 1961, Pub.A.S.P., 73, 292.

Vladimirsky, V. V. 1948, Zhur. Ekap. Theor. Fiz., 18, 392.

Walker, M. F. 1954. Pub.A.S.P., 66, 230.

Walker, M. F. 1957, Non-Stable Stars, ed. G. H. Herbig (Cambridge: Cambridge University Press) p. 46.

Westfold, K. C. 1958, Ap.J., 130, 241.

Willstrop, R. V. 1960, M.N., 121, 17.

Woltjer, L. 1958, B.A.N., 14, 39.

ADDENDUM TO THIS PAPER

VIII. 3C 48 AS A GALAXY

After this paper had been submitted, new evidence strongly suggests that 3C 273, another similar object, has an appreciable redshift ($z = 0.158$, Schmidt 1963). The spectrum of 3C 48 can also be understood if it also has a redshift (Greenstein and Matthews 1963). This section has been included to discuss the observational data for 3C 48 under the assumption that it is a galaxy.

A. The redshift of $z = 0.3675$ for 3C 48 (Greenstein and Matthews 1963) can be interpreted as a distance of 1100 Mpc using a Hubble constant of $H = 100$ km/sec $(\text{Mpc})^{-1}$. Using this distance to calculate the absolute magnitude of the optical object gives the value in Table 9 which has been corrected for the effects of the redshift* but not for interstellar absorptions, except for Cygnus A. The absolute magnitudes for 3C 48 and 3C 273 are compared to other more normal radio galaxies 3C 295 and Cygnus A and to the brightest field and cluster galaxies known (Humason et al 1956). 3C 48 is about 2 magnitudes brighter optically than the brightest field and cluster galaxies, and 2.6 magnitudes brighter than the average of 3C 295 and Cygnus A. Table 9 shows that 3C 273 is even brighter.

The observed radio and optical size of 3C 48 of $\lesssim 1$ second of arc means that the radio and optical flux is coming from a diameter of $\lesssim 5500$ pc. In the case of 3C 273 (Hazard et al 1963; Schmidt 1963), the diameter of the core of component B is $\lesssim 1000$ pc. The faint nebulosity visible around 3C 48 is 66 kpc long if at 1100 Mpc. The nebulosity is probably not a faint underlying galaxy for several reasons. (1) It is much larger than one would expect for a galaxy at that distance. (2) The appearance of the nebulosity does not resemble a galaxy in outline or in the distribution of brightness. (3) The bright object having a stellar appearance on direct plates is not centrally

---

*The bolometric magnitude must be corrected for the K effect due to the shift of the spectrum under the measuring bands. This is composed of two terms, one due to the change of band width of the filters relative to the spectrum being measured, and the other due to the wavelength dependent effect of reducing hertrochromatic magnitudes to bolometric (see eq. B7 of Humason et al 1956). For an effective index of $n = 2$, the second term is zero. The first term is always $2.5 \log (1+z)$. Hence since $n \approx 1.5$ for 3C 48, we neglect the 0^{m}34 for 3C 48. For 3C 295 and Cygnus A, the K correction of Humason et al Table BIII was applied. These corrections are only approximate for two reasons: 1) only the first term (cz/H) in the distance equation (Sandage 1961, eq. 50) has been used; and (2) the selective K term is not known exactly. However, they suffice for our present purpose. Except for Cygnus A, no correction for absorption in our own galaxy has been applied.

located (see Section II). It is 16 kpc from the center of the visible nebulosity. (4) The integrated apparent magnitude of the nebulosity omitting the "star" is $m_v \approx 18.7$. Its absolute magnitude, given in Table 9, is brighter than the brightest of known cluster galaxies, and 1 magnitude brighter than the average of 3C 295 and Cygnus A which are normal radio galaxies. In the case of more normal and radio galaxies, the nucleus of the galaxy is usually the brightest part and contributes significantly to the absolute magnitude. The integrated absolute magnitude for the nebulosity around 3C 48 does not include the effect of any such nucleus.

If the nebulosity was produced by some phenomenon (say an explosion) at some time in the past, then from its visible extent we can infer that the event occurred $\gg 1.8 \times 10^5$ years ago. The minimum corresponds to assuming that the expansion has occurred at the velocity of light and there are no projection effects.

B. Physical Parameters. The physical parameters for 3C 48 at a distance of 1.1×10^9 pc have been computed in exactly the same manner as in Section IV. The results are given in Table 10. Note that the value of the magnetic field for minimum total energy is near 10^{-3} gauss, much lower than suggested in Section IV, and not far from other radio galaxies (Maltby et al 1963). The total energies required are also similar to, but lower than, some of the other radio galaxies. However, note that the time scales are all very short compared to the 1.8×10^5 years suggested above. We can resolve this difficulty in one of two ways. (1) The nuclear region of the galaxy has been continuously producing high energy particles throughout its life time. The total energy required since birth is then 5×10^{59} erg ($\nu_2 = 10^{10}$) or 3×10^{61} erg ($\nu_2 = 5 \times 10^{14}$). (2) The magnetic field is lower by at least the amount required to make the lifetime equal to 1.8×10^5 years. The physical parameters required, under this latter hypothesis, are given in the last row of Table 10. There is no dependance on the size of the object. The total energy required in both these cases is becoming uncomfortably large and it will be even larger if H is made any smaller.

C. Optical Fluctuations. The observation of the optical flux variations (Section III) becomes more important if these objects are galaxies, since we normally do not think of the light from galaxies as varying. A time scale of 6 months for the variations implies a size of the emitting region of $\leqslant 0.15$ pc on the basis of light travel time across the object. If we are seeing statistical variations of a number of similar events, about 10 such events would be happening simultaneously and the emission region would be at least 10 times larger. The variations could still be due to decay of optical synchrotron electrons in a magnetic field of ~ 1 gauss (see Section III). This is not inconsistant when we note that the total energy depends very little on which hypothesis we use in the previous subsection. Thus without changing the total energy requirements very much, we can choose the magnetic field and adjust the emitting volume to fit. The discussion of the lack of radio fluctuations would be the same as in Section III.

REFERENCES

Greenstein, J. L., and Matthews, T. A. 1963, Nature, 197, 1041.

Hazard, C., Mackey, M. B., and Shimmins, A. J. 1963, Nature, 197, 1037.

Humason, M. L., Mayall, N. U., and Sandage, A. R. 1956, A. J., 61, 97.

Sandage, A. R. 1961, Ap. J., 133, 355.

Schmidt, M. 1963, Nature, 197, 1040.

TABLE 9

Absolute Magnitudes Based on H = 100 km/sec 10^6 psc

Object	cz (km/sec)	m_V †	M_V *
3C 48	110,000	16.2	-24.3
Neb 3C 48	110,000	18.7	-22.8
3C 273	47,500	12.6	-25.6
Cyg A	16,830	14.1	-22.1
3C 295	138,000	20.9	-21.3
Field and Cluster†	---	--	-22.3

† On the system of the first brightest.

‡ Not including K correction. For Cyg A includes $1^m.35$ absorption and $0^m.75$ incompleteness.

* Includes K correction.

TABLE 10

Physical Parameters for 3C 48 at the Distance $\frac{cz}{H}$

		$\nu_2 = 10^{10}$ c/s				$\nu_2 = 5\times10^{14}$ c/s			
Size	V (cm^3)	L ($\frac{erg}{sec}$)	H (gauss)	E_T (erg)	τ (year)	L $\frac{erg}{sec}$	H (gauss)	E_T (erg)	τ (year)
S=1"	2.4×10^{66}	3.82×10^{44}	9.1×10^{-4}	1.8×10^{59}	6.4×10^{4}	2.01×10^{46}	1.0×10^{-3}	2.4×10^{59}	1.6×10^{3}
S=0".1	2.4×10^{63}	3.82×10^{44}	6.6×10^{-3}	9.4×10^{57}	3.3×10^{3}	2.01×10^{46}	7.6×10^{-3}	1.2×10^{58}	83
		3.82×10^{44}	2.9×10^{-4}	1.0×10^{60}	1.8×10^{5}	2.01×10^{46}	2.9×10^{-5}	5.3×10^{61}	1.8×10^{5}